International Journal of Solids and Structures 47 (2010) 2097–2114

Contents lists available at ScienceDirect

International Journal of Solids and Structures

journal homepage: www.elsevier.com/locate/ijsolstr

Discrete material optimization of vibrating laminated composite plates for minimum sound radiation

Bin Niu [a,b], Niels Olhoff [a,*], Erik Lund [a], Gengdong Cheng [b]

[a] Department of Mechanical Engineering, Aalborg University, DK-9220 Aalborg, Denmark
[b] State Key Laboratory of Structural Analysis for Industrial Equipment, Dalian University of Technology, 116024 Dalian, China

ARTICLE INFO

Article history:
Received 25 November 2009
Received in revised form 8 April 2010
Available online 6 May 2010

Keywords:
Design optimization of composites
Laminated composite plates
Discrete material optimization
Sound power radiation
Structural–acoustic analysis and optimization

ABSTRACT

This paper deals with vibro-acoustic optimization of laminated composite plates. The vibration of the laminated plate is excited by time-harmonic external mechanical loading with prescribed frequency and amplitude, and the design objective is to minimize the total sound power radiated from the surface of the laminated plate to the surrounding acoustic medium. Instead of solving the Helmholtz equation for evaluation of the sound power, advantage is taken of the fact that the surface of the laminated plate is flat, which implies that Rayleigh's integral approximation can be used to evaluate the sound power radiated from the surface of the plate. The novel Discrete Material Optimization (DMO) formulation has been applied to achieve the design optimization of fiber angles, stacking sequence and selection of material for laminated composite plates. Several numerical examples are presented in order to illustrate this approach.

1. Introduction

Composite materials like fiber reinforced polymers (FRPs) are being used increasingly in aerospace vehicles, maritime carriers, wind turbine blades, and various mechanical equipment where high strength, high stiffness and low weight are important properties. In such applications, the FRPs are usually stacked in a number of layers, each consisting of strong fibers bonded together by a resin, to form a laminate. In addition, laminated sandwich structures may also consist of layers made of foam material. When these composite structures are used in dynamic environments, vibration control and noise reduction become of great technical significance. In the present paper, this design objective will be considered in the form of minimizing the sound radiation from a laminated composite plate. This is accomplished by optimizing simultaneously the laminates in terms of proper choice of material, stacking sequence and fiber orientation. Such advanced optimization of laminates has only recently become possible via development of optimization approaches such as the method of Discrete Material Optimization (DMO) in the papers (Stegmann and Lund, 2005; Lund and Stegmann, 2005), and practically feasible via new developments in the manufacture of composite materials and structures.

Excellent textbooks on optimization for passive design of structural–acoustic systems against vibration and noise (Koopmann and Fahnline, 1997; Kollmann, 2000), and the proceedings of an IUTAM Symposium on design for quietness (Munjal, 2002), were already published about 10 years ago. These publications as well as papers like (Pedersen, 1982; Olhoff and Parbery, 1984; Bendsøe and Olhoff, 1985; Christensen et al., 1998a,b; Sorokin et al., 2006; Bös, 2006) did not specially address composite structure applications, but provide an overview and contain references to the area of design optimization with respect to acoustic criteria in general.

However, as mentioned above, structural–acoustic optimization of composite structures has received increasing attention with the extensive application of composite materials in recent years, and in terms of optimization of composite structures with respect to acoustic criteria, we may refer the reader to the review article (Denli and Sun, 2007) and the bibliography (Mackerle, 2003), and a large number of papers cited therein. As examples of various types of problems of optimum structural–acoustic design with composite materials, we may refer to (Hufenbach et al., 2001; Thamburaj and Sun, 2002; Chen et al., 2005; Yamamoto et al., 2008; Jensen, 2009).

Relative to sizing or shape optimization, structural topology optimization generally yields a more efficient conceptional/configurational design at the stage of initial design. In 1988, Bendsøe and Kikuchi (1988) implemented the topology optimization of continuum structures via a homogenization method and laid the foundation of modern structural topology optimization, and this type of optimization has been an extremely active area of research since then. For the state-of-the-art in topology optimization the reader is referred to the review article (Eschenauer and Olhoff, 2001), the exhaustive textbook (Bendsøe and Sigmund, 2003), the paper

* Corresponding author.
E-mail address: no@ime.aau.dk (N. Olhoff).

0020-7683/$ - see front matter © 2010 Elsevier Ltd. All rights reserved.
doi:10.1016/j.ijsolstr.2010.04.008

(Bendsøe et al., 2005), and the proceedings from an IUTAM Symposium (Bendsøe et al., 2006).

Up to now, the method of topology optimization has been mainly applied to three classes of problems within the area of structural–acoustic design, however with no particular focus on composite structure applications. The first class of problems encompasses maximization of intrinsic properties of the structures like fundamental and higher order eigenfrequencies, gaps between two consecutive eigenfrequencies, and phononic band gaps, see, e.g. (Dias and Kikuchi, 1992; Bendsøe and Diaz, 1994; Ma et al., 1995; Kosaka and Swan, 1999; Krog and Olhoff, 1999; Pedersen, 2000; Sigmund, 2001; Tcherniak, 2002; Jensen, 2003; Sigmund and Jensen, 2003; Olhoff and Du, 2005; Diaz et al., 2005; Jensen and Pedersen, 2006; Halkjær et al., 2006; Du and Olhoff, 2007b; Mendonca et al., 2009; Akl et al., 2009). The second class of problems comprises minimization of the dynamic compliance, i.e., maximization of the dynamic stiffness, of structures subjected to forced vibration by time-harmonic external mechanical loading of given frequency (or frequency range), see, e.g. (Min et al., 1999; Jog, 2002a,b; Calvel and Mongeau, 2005; Jensen, 2007; Olhoff and Du, 2010). Finally, the third class of structural–acoustic topology design problems includes minimization of the acoustic power radiated from the structural surface(s) into a surrounding or interior acoustic medium like air, when the structure is subjected to forced vibration by time-harmonic external mechanical loading of given frequency or frequency range, see, e.g., the papers (Luo and Gea, 2003; Wadbro and Berggren, 2006; Yoon et al., 2007; Du and Olhoff, 2007a, 2010; Dühring et al., 2008; Olhoff and Du, 2008).

It is worth noting (Olhoff and Du, 2008) that the design objectives of the above-mentioned three classes of structural–acoustic topological design optimization problems generally have the same mechanical effect. This effect consists in driving the nearest resonance frequencies of the structure as far away as possible from a given external excitation frequency, or a band of excitation frequencies; this way structural resonance phenomena with high vibration and noise emission levels are avoided by the optimization.

Through structural topology optimization, composite structures can be tailored to optimally achieve certain objectives. In the present paper, the objective is to minimize the acoustic power radiated from vibrating composite structures. An efficient and reliable numerical design tool is very important in order to realize the topology optimization of vibrating laminated composite plates, and the novel Discrete Material Optimization (DMO) formulation proposed in Stegmann and Lund (2005) and Lund and Stegmann (2005) has been applied to achieve this goal.

The optimization of fiber orientation in composite laminates was first considered by Rasmussen (1979), see Niordson and Olhoff (1979). Several other methods have already been proposed to realize optimum fiber orientation problems for orthotropic materials: optimality criteria for orientational design (Pedersen, 1989, 1991; Cheng and Pedersen, 1997), parameterization based on lamination parameters (Miki and Sugiyama, 1993), a general approach of forcing convexity of ply angle optimization based on lamination parameters (Foldager et al., 1998), and an energy based method (Luo and Gea, 1998) for the optimum orientation problem. The optimization of fiber orientation and concentration of one or two fiber fields in composite laminates is dealt with in Thomsen and Olhoff (1990), Thomsen (1991), where cross-ply fiber reinforcement is allowed for. As opposed to these methods of optimization of fiber orientation, DMO is based on ideas from multiphase topology optimization (Sigmund and Torquato, 1997) to achieve a parameterization. Thus, DMO lends itself to the methodology of topology optimization, and the method has proven to reduce the risk of obtaining local optimum solutions for fiber orientations, and to be able to solve simultaneously the optimization of materials, stacking sequence and fiber orientations, using a predefined set of discrete candidate materials and fiber angles as design variables at element level.

It is assumed in this paper that air is the acoustic medium and that a feedback coupling between the acoustic medium and the structure can be neglected. Rayleigh's integral is used for computation of the sound power radiated from the structural surface instead of solving the Helmholtz integral equation. This implies that the computational cost of the structural–acoustic analysis can be considerably reduced, which is very efficient for the design optimization. It has been proved that Rayleigh's integral provides a very good approximation of the sound pressure distribution along a relatively flat structural surface, see Lax and Feshbach (1947), Herrin et al. (2003), and Du and Olhoff (2007a).

The organization of the remainder of this paper is as follows. In Section 2, the problem of structural topology optimization of laminated composite plates subject to given amounts of the constituents is formulated for the objective of minimizing the sound power radiated from the vibrating structural surface into the acoustic medium. Then Rayleigh's integral is introduced to calculate the sound power flow from the structural surface, which leads to a simplified optimization formulation of the current problem. Section 3 introduces the parameterization for Discrete Material Optimization (DMO) and discusses penalty functions for DMO. Section 4 presents a DMO convergence measure. Section 5 deals with the sensitivity analysis required for the numerical optimization algorithm. Section 6 outlines several numerical examples with different excitation frequencies in order to validate the proposed method, including single-layer, multi-layer laminated composite plates, and laminated sandwich plates consisting of layers made of FRPs and foam material. In Section 7, two isotropic materials are introduced together with unidirectional fiber material as candidate materials in single-layer plate design. Finally, a section with conclusions closes the paper.

2. Minimization of sound power radiation for laminated composite plate using Discrete Material Optimization (DMO)

We consider design optimization of vibrating laminated composite plates with the objective of minimizing the total sound power (energy flux) Π radiated from the structural surface S into a surrounding acoustic medium. The same objective has been applied in Du and Olhoff (2007a) for a vibrating isotropic bi-material elastic plate. The present work aims to realize this objective for a laminated composite plate by design optimization of stacking sequence, fiber orientations, and selection of layer materials. This problem is solved by using the so-called Discrete Material Optimization (DMO) approach in the sense that the structural constituents are chosen from among a given set of different candidate materials (Stegmann and Lund, 2005), which may be regarded as an extension of classical topology optimization (see, e.g., Bendsøe and Sigmund, 2003; Rozvany et al., 1992) with a constraint on the total volume of material.

The mathematical formulation of the problem is as follows.

$$
\begin{aligned}
&\min_{\mathbf{x}} \left\{ \Pi = \int_S I_n \, dS = \int_S \frac{1}{2} Re(p_f v_n^*) dS \right\} \\
&\text{s.t.} \quad (\mathbf{K} - \omega_p^2 \mathbf{M})\mathbf{U} = \mathbf{P} + \mathbf{L}\mathbf{P}_f \\
&\qquad \mathbf{C}_\alpha \mathbf{P}_f = \mathbf{G}\mathbf{U} - \mathbf{H}\mathbf{P}_f \\
&\qquad \sum_{e=1}^{N^e} \left(\sum_{l=1}^{N^l} \sum_{i=1}^{n^l} (\xi_{eli} u_i) t_l \right) A_e \leqslant \overline{R} \\
&\qquad 0 < x_{\min} \leqslant x_j \leqslant x_{\max} < 1, \quad j = 1, N^{dv}
\end{aligned}
\tag{1}
$$

In the expression for the total radiated sound power Π in (1), the symbols p_f and v_n^* represent the acoustic pressure and the complex conjugate of the normal velocity of the structural surface, and $\mathbf{P}_f$ denotes the corresponding vector of amplitudes of the acoustic pressure on the structural surface S. The symbol **L** represents the fluid–structural coupling matrix. The matrices **G**, **H** and $\mathbf{C}_\alpha$ can be generated by the discretized Helmholtz integral and calculation of the spatial angle along the structural surface (see, e.g., Christensen et al., 1998a,b), and **P** denotes the vector of amplitudes of a given external time-harmonic mechanical loading vector $\mathbf{p}(t) = \mathbf{P}e^{i\omega_p t}$ with the prescribed excitation frequency ω_p. The symbols **K** and **M** represent the global structural stiffness and mass matrices, **U** denotes the vector of magnitudes of the corresponding structural displacement response vector $\mathbf{a}(t) = \mathbf{U}e^{i\omega_p t}$, and $\mathbf{K}_d = (\mathbf{K} - \omega_p^2\mathbf{M})$ is defined as the global dynamic stiffness matrix. Here, **M** depends on the mass density γ_i of each of the candidate materials, $i = 1,2,\ldots$, and it is assumed that damping can be neglected.

Since laminated composite plates are considered, more design parameters need to be introduced as compared to single material solid plates. Thus, l denotes "layer", e denotes "element", N^l is the number of layers, N^e is the number of elements, and n^l is the number of candidate materials (design variables) per layer for each element; the number of element design variables n^e for multi-layered elements (with N^l layers) is the sum of the number of design variables per layer, n^l, over all N^l layers, such that $n^e = \sum_{k=1}^{N^l} n_k^l$, and the total number of design variables in the problem is therefore $N^{dv} = \sum_{i=1}^{N^e} n_i^e$. It is emphasized that the "classical" topology optimization formulation has one design variable per element by setting $n^e = 1$ for single material 0/1 design. For single-layer plates, the number of candidate materials is also the number of element design variables. Here we consider a more general condition with multiple layers, where the number of design variables must be summed over all layers for this element. The symbol t_l and A_e represent the thickness of the l-th layer and area of the e-th element, respectively. In the DMO approach, the variable x_i ($i = 1,2,\ldots,n^l$) per layer for each element can be seen as a local density variable that indicates possible selection of the i-th material, i.e., with $x_i = x_{\max}$ meaning that the i-th material is chosen and $x_i = x_{\min}$ meaning that the i-th material is not chosen. The design variables **x** for all layers in all elements are denoted as

$$\mathbf{x} = \{x_j \,|\, j = e \times l \times i, \text{ where } e = 1,2,\ldots,N^e; l = 1,2,\ldots,N^l; \; i = 1,2,\ldots,n^l\} \tag{2}$$

Thus, in comparison with classical topology optimization of a single material structure, an extended parameterization is invoked in the DMO approach which enables penalization of intermediate values of the design variables such that a distinct choice of candidate material may be made. The symbol ξ_{eli} denotes the weighting function of the i-th candidate material in the l-th layer of the e-th element in the parameterization of the Discrete Material Optimization (DMO) formulation, see the subsequent section for a detailed definition. For the sake of brevity, we use subsequently in Sections 3–5 the symbol ξ_i instead of ξ_{eli} to denote the weighting functions in a certain layer of a certain element without special statements. More discussion on weighting functions of DMO can be found in Stegmann and Lund (2005).

The symbol $\overline{R}$ in (1) denotes the given resource, which enforces an upper bound for the total cost or mass of the structure. The symbol u_i is defined as a so-called "unit cost factor" of the i-th candidate material. Accordingly, for a cost or a mass constrained problem, u_i represents the cost c_i or the mass γ_i per unit volume of the i-th candidate material in this paper. For the problem of pure fiber angle optimization, the resource constraint may be left out entirely when the unit cost factors for all unidirectional fiber materials are assumed equal, because a change in fiber angle does not influence the total cost or mass. However, this constraint on resource needs to be considered when multiple material optimization is implemented, e.g., foam material introduced as candidate material together with unidirectional fiber material. The notion of unit cost factors has been used earlier in the context of other structural optimization problems; see, for example, Taylor (1975), Mroz and Rozvany (1975), Prager (1977a,b), Olhoff and Taylor (1978), and Olhoff and Taylor (1979).

In the problem formulation (1), the structural–acoustic coupling occurs due to the appearance of the acoustic surface pressure vector $\mathbf{P}_f$ and the structural displacement response vector **U** in both the first and second constraint equation in (1), i.e., the equation for forced structural vibration without damping and the discretized Helmholtz integral equation for the acoustic medium. Now, direct solution of the Helmholtz integral equation implies large computational cost, and the equation has to be solved together with the structural equation in each iterative step of the optimization process. Therefore, for simplification, Rayleigh's integral approximation is adopted for determining the acoustic pressure distribution and sound power radiation.

The conditions for this are that the structure is flat, which is clearly met by the laminated plates considered, and that the prescribed excitation frequency ω_p is sufficiently high or the observation points are sufficiently far away from the laminated plate, such that the product kr is much larger than 1, where $k = \omega_p/c$ is the wave number, c the speed of sound in the acoustic medium, and r is the distance between a source point on the structural surface and an observation point in the acoustic domain, cf. Herrin et al. (2003). Following (Du and Olhoff, 2007a), assuming a sufficiently high value of the structural vibration frequency ω_p, the radiation impedance p_f/v_n at the structural surface will be approximately equal to the characteristic impedance $\gamma_f c$ of the acoustic medium (Lax and Feshbach, 1947). Thus, the acoustic pressure p_f and the normal velocity v_n of the structural surface are approximatively related by the simplified equation

$$p_f = \gamma_f c v_n \tag{3}$$

where γ_f is the mass density and c the sound speed in the acoustic medium. The accuracy of the approximation is discussed in the papers (Du and Olhoff, 2007a) and Herrin et al. (2003).

The normal velocity of the surface in (3) can be obtained as

$$v_n = \mathbf{n} \cdot \mathbf{u} \cdot (i\omega_p) \tag{4}$$

where **n** is the unit normal and **u** the amplitude of the displacements of the structural surface after interpolation based on finite element analysis, i.e., using the finite element interpolation $\mathbf{u} = \mathbf{N}\mathbf{U}_e$, where **N** is the shape function and $\mathbf{U}_e$ is the nodal displacement vector of element e.

Thus, substituting (3) with v_n given by (4) into the expression for the sound power (objective function) Π in (1), we after simple algebra obtain the simplified expression

$$\Pi = \int_S \frac{1}{2}\gamma_f c\omega_p^2 (\mathbf{n}\cdot\mathbf{u})(\mathbf{n}\cdot\mathbf{u}) dS \tag{5}$$

which upon use of the discretized formulations can be written in the matrix form

$$\Pi = \frac{1}{2}\gamma_f c\omega_p^2 \mathbf{U}^T \mathbf{S}_n \mathbf{U} \tag{6}$$

where superscript T stands for transpose, **U** denotes the global displacement vector of the structure, and $\mathbf{S}_n$ defined as

$$\mathbf{S}_n = \sum_{e=1}^{N^e} \mathbf{S}_{ne} = \sum_{e=1}^{N^e} \left(\int_{S_e} \mathbf{N}^T \mathbf{n}\mathbf{n}^T \mathbf{N} dS \right) \tag{7}$$

is termed the surface normal matrix of the structure.

Finally, in this paper we shall consider the acoustic medium to be light, i.e., air with the mass density $\gamma_f = 1.2\ \mathrm{kg/m^3}$ and sound speed $c = 343.4$ m/s. This means that we may assume weak coupling, i.e., ignore the acoustic pressure on the structure, and this implies a further simplification of the current optimization problem. All in all, with the simplifications made, the original formulation (1) of our optimization problem can be re-written in the very convenient form

$$\begin{aligned} &\min_{\mathbf{x}} \Pi = \frac{1}{2}\gamma_f c\omega_p^2 \mathbf{U}^T \mathbf{S}_n \mathbf{U} \\ &\text{s.t.} \quad (\mathbf{K} - \omega_p^2 \mathbf{M})\mathbf{U} = \mathbf{P} \\ &\qquad \sum_{e=1}^{N^e} \left(\sum_{l=1}^{N^l} \sum_{i=1}^{n^l} (\xi_{eli} u_i) t_l \right) A_e \leqslant \overline{R} \\ &\qquad 0 < x_{\min} \leqslant x_j \leqslant x_{\max} < 1, \quad j = 1, N^{dv} \end{aligned} \tag{8}$$

When comparing (8) with (1), let us first note that the assumption of weak coupling implies that the feedback acoustic pressure $\mathbf{LP}_f$ on the structure in (1) vanishes such that the first constraint in (8) is simply the standard equation for a vibrating structure without damping, that is subjected to the given external dynamic loading $\mathbf{P}$, only. At the same time, in (8) the Rayleigh approximation (3) has dismissed the discretized Helmholz integral equation in the second constraint in (1) and instead taken over itself the delivery of acoustic surface pressures to Π (cf. the expression for Π in (1)), and finally substituted these pressures by surface normal velocities converted into global structural displacements $\mathbf{U}$ in the expression for Π in (8). We notice that these displacements $\mathbf{U}$ are simply obtained by solution of the standard equation for forced vibration of the structure in the first constraint of (8).

We may conclude that the application of Rayleigh's approximation and the assumption of weak coupling have furnished a formulation (8) of our optimization problem that is much simpler than the formulation in (1) based on Helmholtz' integral equation and full structural–acoustic coupling. Thus, problem (8) does not require a system of coupled equations (the first and second constraint equations in (1)) to be assembled and solved, and it must therefore be much easier to implement, much faster to solve numerically, and require considerably less computer resources than problem (1). Similar advantages must be expected for the sensitivity analysis of problem (8).

3. DMO parameterization model for topology optimization of multi-layer structures

The DMO method (Stegmann and Lund, 2005; see the thesis Stegmann, 2004 for further details) achieves a parameterization as an extension of the ideas used in structural topology optimization (Bendsøe and Kikuchi, 1988). Thus, instead of choosing between solid and void, the DMO method realizes the ability to choose from among a given number of candidate materials. Hereby, the DMO formulation extends the scope of application of multiphase topology optimization (Sigmund and Torquato, 1997) and allows the structures to be multi-layered and made of orthotropic materials.

The element constitutive matrix per layer is expressed as a weighted sum of the matrices of the candidate materials. Various parameterization schemes have been developed in Stegmann and Lund (2005) and Stegmann (2004) for discrete material optimization (DMO), see also Lund and Stegmann (2005) and Lund (2009). For multi-layer structures, the interpolation method must be implemented layer-wise for each element, i.e. for all layers in all elements. Consequently, the interpolation scheme is written by layer, and the constitutive relation for the l-th layer has the form

$$\mathbf{Q}^l = \sum_{i=1}^{n^l} \xi_i \mathbf{Q}_i = \xi_1 \mathbf{Q}_1 + \xi_2 \mathbf{Q}_2 + \cdots + \xi_{n^l} \mathbf{Q}_{n^l} \tag{9}$$

where each candidate material is characterized by a constitutive matrix $\mathbf{Q}_i$. The weighting functions ξ_i must all attain values between 0 and 1 in order to be physically acceptable. Furthermore, it is found to be necessary that the sum of the weighting functions is always one, i.e. $\sum_{k=1}^{n^l} \xi_k = 1$, which is important for a physical interpretation of the designs and for correct evaluation of quantities such as the mass, weight and cost, etc. In Eq. (9), the parameterization model is realized element-wise for single-layers and layer-wise for multiple layers for a large number of candidate materials.

In this paper, a DMO parameterization is used which enforces unit value of the sum of the weighting functions. The weighting functions can be expressed as

$$\xi_i = \sum_{i=1}^{n^l} \frac{\bar{\xi}_i}{\sum_{k=1}^{n^l} \bar{\xi}_k} \tag{10}$$

where

$$\bar{\xi}_i = (x_i^l)^p \prod_{j=1; j \neq i}^{n^l} [1 - (x_j^l)^p] \tag{11}$$

Here the unity demand is realized by normalizing each weighting function initially computed by Eq. (11). It has been noted that the effect of the penalized intermediate values of the weighting functions is slightly reduced when introducing the normalization. The weighting functions ξ_1 and ξ_2 are illustrated in Fig. 1(a) and (b) for unit value of the penalty factor p, and the sum of them is shown in Fig. 1(c). It is found that the sum of the weighting functions attains unit value for any combination of intermediate values of design variables. For a value of the penalty factor p larger than unity, e.g., $p = 3$, the weighting functions ξ_1 and ξ_2 are shown in Fig. 2(a) and (b), and the sum of them again attains unit value as indicated in Fig. 2(c). The increase of the penalty factor slightly increases the size of the flat triangle-like plateau and the slope in the center is steeper. This implies that the increase of the penalty factor will not help too much to penalize intermediate values of the design variables. Fig. 3(a)–(c) depicts the weighting functions ξ_1,ξ_2 and their sum if the penalty factor is further increased up to the value $p = 10$. The differences between Figs. 1 and 3 are seen to be more significant. We note that the two plateau domains in Fig. 3(a) and (b) are not favourable for penalization of design variables with values located in these two domains. Due to this, the power p is typically increased gradually from 1 to 3 only, and not up to a higher value during the continuation process.

Similarly, the element mass density and element cost per layer, i.e. for the l-th layer, are also expressed as a weighted sum for the candidate materials, respectively,

$$\gamma^l = \sum_{i=1}^{n^l} \xi_i \gamma_i = \sum_{i=1}^{n^l} \frac{\bar{\xi}_i}{\sum_{k=1}^{n^l} \bar{\xi}_k} \gamma_i \tag{12}$$

$$c^l = \sum_{i=1}^{n^l} \xi_i c_i = \sum_{i=1}^{n^l} \frac{\bar{\xi}_i}{\sum_{k=1}^{n^l} \bar{\xi}_k} c_i \tag{13}$$

where γ_i denotes the mass density and c_i the unit cost of the i-th candidate material. The weighting functions ξ_i use the same interpolation formulae in Eq. (10).

For the resource constraint, linear interpolation is used, which means that the penalty power $p = 1$. However, for the stiffness and mass matrices, nonlinear interpolation is used, and the penalty power p is typically increased gradually from 1 up to 3.

Furthermore, the element stiffness and mass matrices can be obtained on the basis of first-order laminated composite plate the-

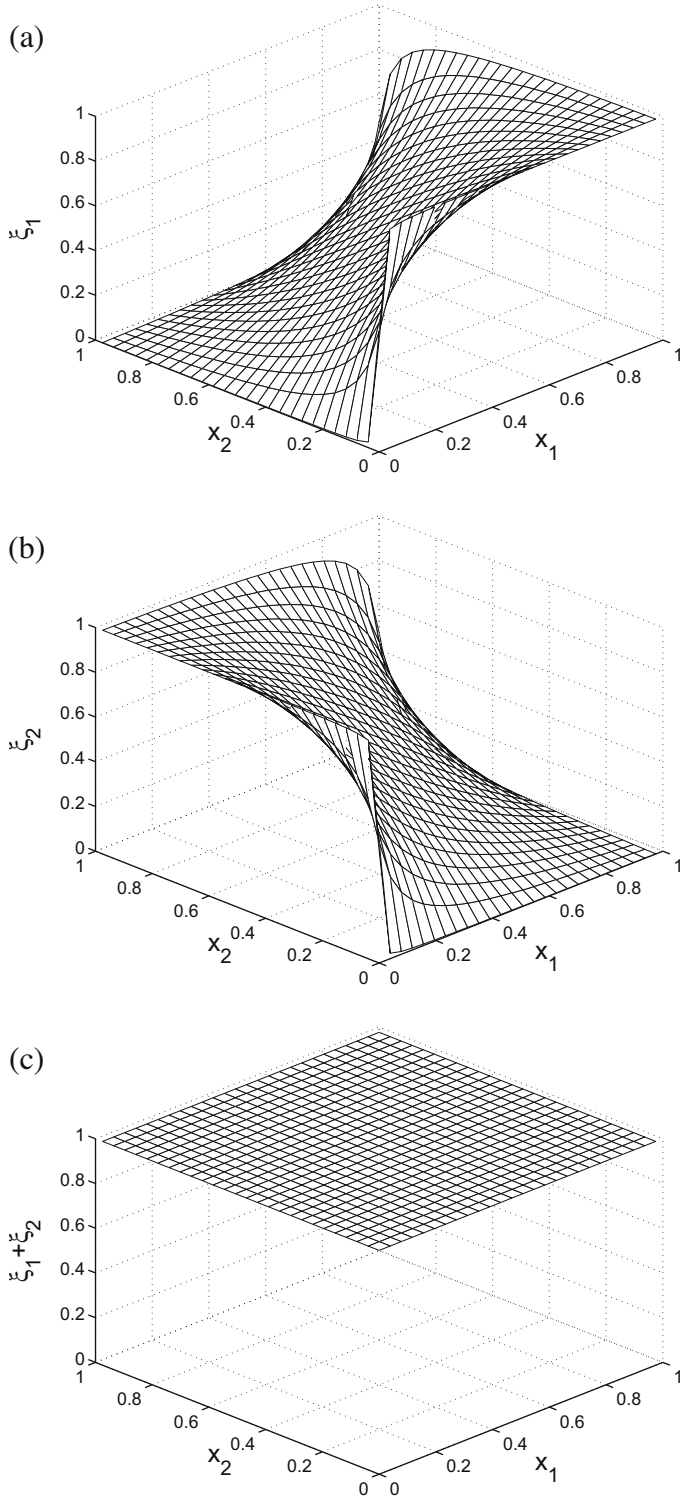

Fig. 1. Weighting functions ξ_1 and ξ_2, and the sum of them for two materials with the penalty factor $p = 1$.

ory, and the global stiffness and mass matrices can be obtained by assembling the element matrices.

4. Evaluation of convergence

A convergence measure given in Stegmann and Lund (2005) is adopted to describe whether the optimization has converged to a satisfactory result. This convergence measure is described briefly here, while the reader is referred to the original paper (Stegmann and Lund, 2005) for a detailed discussion. For each layer in each element the inequality is evaluated for all weighting functions, ξ_i

$$\xi_i \geqslant \varepsilon\sqrt{\xi_1^2+\xi_2^2+\cdots+\xi_n^2} \tag{14}$$

where ε is a tolerance level, typically 95–99.5% suggested by Stegmann and Lund (2005). If the inequality is satisfied for one of the weighting functions in the layer, it is flagged as converged. The DMO convergence measure h_ε is defined as the ratio between the number of converged layers $N_c^{l,tot}$ in all elements and the total number of layers in all elements $N^{l,tot} = N^l \cdot N^e$

$$h_\varepsilon = \frac{N_c^{l,tot}}{N^{l,tot}} \tag{15}$$

The DMO convergence measure is denoted as h_{95} if the tolerance level is 95% and full convergence, $h_{95} = 1$, means that all layers in all elements have a single weighting function contributing more than 95% to the Euclidian norm of the weighting functions.

5. Design sensitivity analysis

The sensitivity of the objective function (i.e., the sound power Π) in formulation (8) with respect to the design variable x_k is given by

$$\frac{\partial \Pi}{\partial x_k} = \frac{\partial\left(\frac{1}{2}\gamma_f c\omega_p^2 \mathbf{U}^T\mathbf{S}_n\mathbf{U}\right)}{\partial x_k} \tag{16}$$

Since the surface normal matrix $\mathbf{S}_n$ is independent of the design variables, we obtain

$$\frac{\partial \Pi}{\partial x_k} = \gamma_f c\omega_p^2 \mathbf{U}^T\mathbf{S}_n\frac{\partial(\mathbf{U})}{\partial x_k} \tag{17}$$

Using the adjoint method (see, e.g. Tortorelli and Michaleris, 1994; Du and Olhoff, 2007a), the sensitivity of the objective function can be obtained in a more efficient manner as

$$\frac{\partial \Pi}{\partial x_k} = \gamma_f c\omega_p^2 \mathbf{U}^T\mathbf{S}_n\frac{\partial(\mathbf{U})}{\partial x_k} = \gamma_f c\omega_p^2\left[-\mathbf{U}_s^T\left(\frac{\partial \mathbf{K}}{\partial x_k}-\omega_p^2\frac{\partial \mathbf{M}}{\partial x_k}\right)\mathbf{U}\right] \tag{18}$$

Here $\mathbf{U}_s$ is the solution to the equation

$$(\mathbf{K}-\omega_p^2\mathbf{M})\mathbf{U}_s = \mathbf{S}_n\mathbf{U} = \mathbf{P}_s \tag{19}$$

where $\mathbf{P}_s$ may be regarded as a pseudo surface load vector.

The sensitivities of the stiffness and mass matrices can be derived by the DMO parameterization model introduced in the previous section.

The global resource constraint in (1) and (8) that specifies an upper bound value $\overline{R}$ for the total cost or mass of the structure, can be transformed into

$$g = \frac{\sum_{e=1}^{N^e}\left(\sum_{l=1}^{N^l}\sum_{i=1}^{n^l}(\xi_{eli}u_i)t_l\right)A_e}{\overline{R}} \leqslant 1 \tag{20}$$

and the sensitivities of the corresponding constraint function g with respect to the design variables are easily obtained as

$$\frac{\partial g}{\partial x_k} = \frac{t_k A_k}{\overline{R}}\sum_{i=1}^{n^l}\left(\frac{\partial \xi_i}{\partial x_k}u_i\right) \tag{21}$$

It should be reiterated that linear interpolation with the penalty factor $p = 1$ is adopted for the resource constraint. With these sensitivity results, the design problem (8) may be solved by a mathematical programming method, e.g., MMA by Svanberg (1987). A broad account of finite element based design sensitivity analysis and optimization is available in Lund (1994).

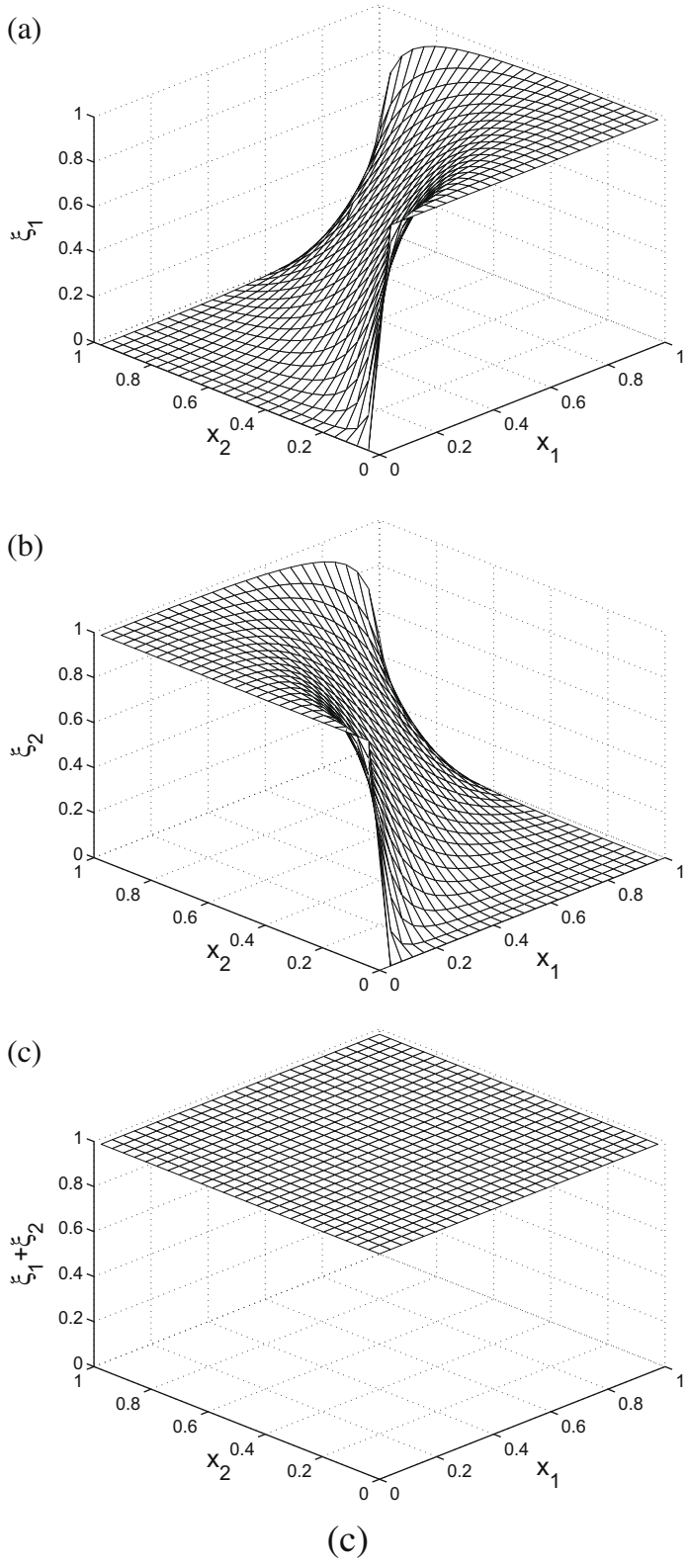

Fig. 2. Weighting functions ξ_1 and ξ_2, and the sum of them for two materials with the penalty factor $p = 3$.

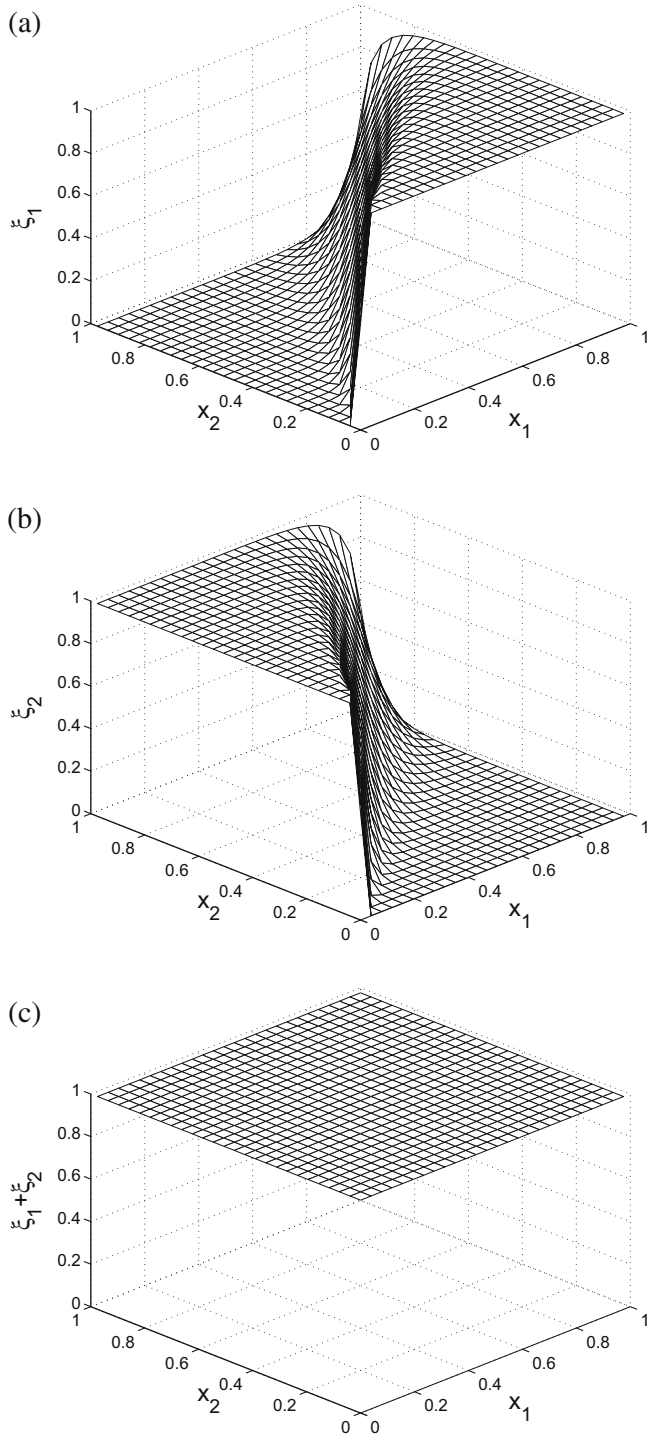

Fig. 3. Weighting functions ξ_1 and ξ_2, and the sum of them for two materials with the penalty factor $p = 10$.

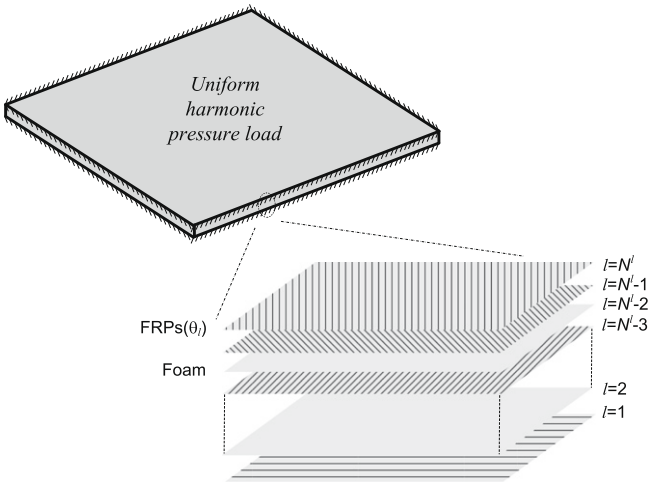

Fig. 4. Quadratic laminated plate structure subjected to uniformly distributed time-harmonic pressure loading. All four plate edges are clamped.

6. Numerical experiments of laminated composite plates: discrete material optimization of single-layer, multi-layer and sandwich plates

6.1. Single-layer plate

Firstly, the problem of a single-layer clamped quadratic plate subjected to uniformly distributed time-harmonic pressure loading $p(t) = P\cos\omega_p t$ with $P = 10^5$ is considered for minimum sound radiation by Discrete Material Optimization (DMO). The side lengths of the plate are 1 m and the thickness t is 0.01 m. All quantities are given in SI units in this paper. Laminated Mindlin plate elements based on first order shear deformation theory are used in the following numerical experiments. A nine-node Mindlin laminated plate element with five degrees of freedom at each node is adopted. An element with this number of degrees of freedom per node is chosen because in several of the examples in this paper, the design parameterization allows for coupling between in-plane and bending deformation, such that the B-matrix in an A–B–D description of the laminate is non-zero. A 20×20 mesh discretization is applied for the plate and it should be noted that symmetry is not invoked in the analysis. We have tested that the finite element mesh used yields sufficiently accurate computational results in the frequency ranges considered. As candidate materials we use a glass/epoxy composite with $E_x = 54$ GPa, $E_y = E_z = 18$ GPa, $G_{xy} = G_{yz} = G_{zx} = 9$ GPa, Poisson's ratio $\upsilon_{xy} = 0.25$ and mass density $\gamma = 1900$ kg m^{-3}. The fiber angles are taken to be [90°, ±45°, 0°].

For all the examples in this paper, unbiased initial values of design variables were set to the value corresponding to uniform distribution of all candidate materials (in this section 0.25). The corresponding initial design provides a convenient reference for evaluation and discussion of the vibration and sound power radiation characteristics of the designs optimized by usage of DMO in the following. In this section the initial design corresponds to a quasi-isotropic layup of the glass/epoxy material. We start out computing a lower spectrum of eigenfrequencies ω_i of the initial design and find the results given in Table 1, where $\omega_2 = \omega_3 = 884$. is a bimodal (double) eigenfrequency.

In Table 1, ω_1 and ω_6 identify the first and second resonance frequency, respectively, denoted as Ω_1 and Ω_2. Thus, it is easily shown that the eigenfrequencies $\omega_2, \omega_3, \ldots, \omega_5$ in both Tables 1 and 2 are

Table 1
Eigenfrequencies ω_i and resonance frequencies Ω_i of the initial design.

ω_1	ω_2	ω_3	ω_4	ω_5	ω_6
434 = Ω_1	884	884	1302	1583	1591 = Ω_2

Table 2
Eigenfrequencies ω_i and resonance frequencies Ω_i of the optimized design associated with the excitation frequency $\omega_p = 500$.

ω_1	ω_2	ω_3	ω_4	ω_5	ω_6
354 = Ω_1	834	834	1181	1415	1492 = Ω_2

not resonance frequencies for the forced time-harmonic vibration problems considered in this section. We recall that the amplitudes of the pressure loading are assumed to be the same all over the plate domain, and when computing the scalar products $\mathbf{P}^T\phi_i$ for i = 2,...,5, where $\mathbf{P}$ is the vector of load amplitudes and ϕ_i are the vectors of the eigenmodes associated with the eigenfrequencies ω_i, $i = 2,\ldots,5$, we find that (within computational accuracy) the scalar product $\mathbf{P}^T\phi_i = 0$ for $i = 2,\ldots,5$. This means that the eigenvectors ϕ_i, $i = 2,\ldots,5$, are orthogonal to the vector of the load amplitude $\mathbf{P}$, and implies that these eigenmodes are not excited by the dynamic loading. Hence, the corresponding eigenfrequencies $\omega_2,\ldots,\omega_5$ are not resonance frequencies of the forced vibration problem, and will not affect the sound power radiation from the structure. Both in Tables 1 and 2, the eigenmodes corresponding to the first and sixth eigenfrequency ω_1 and ω_6, respectively, are found not to be orthogonal to the amplitudes of the dynamic loading, which means that ω_1 and ω_6 constitute the first and the second resonance frequency Ω_1 and Ω_2, respectively, of the forced vibration problem.

For the optimization six prescribed different loading frequencies, $\omega_p = 10$, 100, 200, 300, 500 and 1000 are considered, which cover designs from the low frequency to a lower-medium frequency level (note that the fundamental resonance frequency of the initial design is $\Omega_1 = 434$.). The optimized designs with their fiber orientations are shown in Fig. 5. The optimum design for minimum sound power at the low excitation frequency $\omega_p = 10$ resembles the optimum design for maximum stiffness in Lund and Stegmann (2005). The DMO convergence measures in Eq. (15) of these six results with different excitation frequencies are $h_{95} = 0.82$ for $\omega_p = 10$, $h_{95} = 0.82$ for $\omega_p = 100$, $h_{95} = 0.80$ for $\omega_p = 200$, $h_{95} = 0.80$ for $\omega_p = 300$, $h_{95} = 0.99$ for $\omega_p = 500$ and $h_{95} = 0.98$ for ω_p =1000. The DMO convergence measure is seen to be not very high for the cases with lower values of the excitation frequency. For these cases, it is observed that the not-fully converged elements are mostly located in the narrow central region of the optimized plate. In this region, it is found that the weighting functions associated with unidirectional fiber material oriented at ±45°, 90° and 0° are very close to each other. This issue will be taken up in Section 7. In the optimized designs in Fig. 5, the material with the highest associated weighting function is plotted. Fig. 6 shows the iteration histories behind the optimized designs in Fig. 5(a), (b) and (e) corresponding to the excitation frequencies $\omega_p = 10$, 100 and 500. It is seen that the three curves all exhibit rapid convergence of the sound radiation.

The optimum designs in Fig. 5 are observed to be similar to each other for the excitation frequencies 10, 100, 200 and 300, which are all below the first resonance frequency Ω_1 of the initial design as well as the resulting optimized designs. However, different topologies are found when higher excitation frequencies are considered. The sound power radiation has generally been decreased quite substantially for the optimized design relative to the initial design in all the examples, see Table 3.

As is seen in Table 3, the largest decrease (75.66%) of the sound power emission Π relative to that of the initial design, is obtained for the optimized design in Fig. 5(e) with the prescribed external excitation frequency $\omega_p = 500$. The reason for this large decrease of Π is that $\omega_p = 500$ is quite close to (slightly larger than) the first resonance frequency $\omega_1 = 434$ of the initial design (as is also reflected by the high value of the sound power radiation Π_0 from the initial design at $\omega_p = 500$ in Table 3). Thus, taking the optimized design with $\omega_p = 500$ in Fig. 5(e) to be given, we have computed its six lowest eigenfrequencies and obtained the results shown in Table 2.

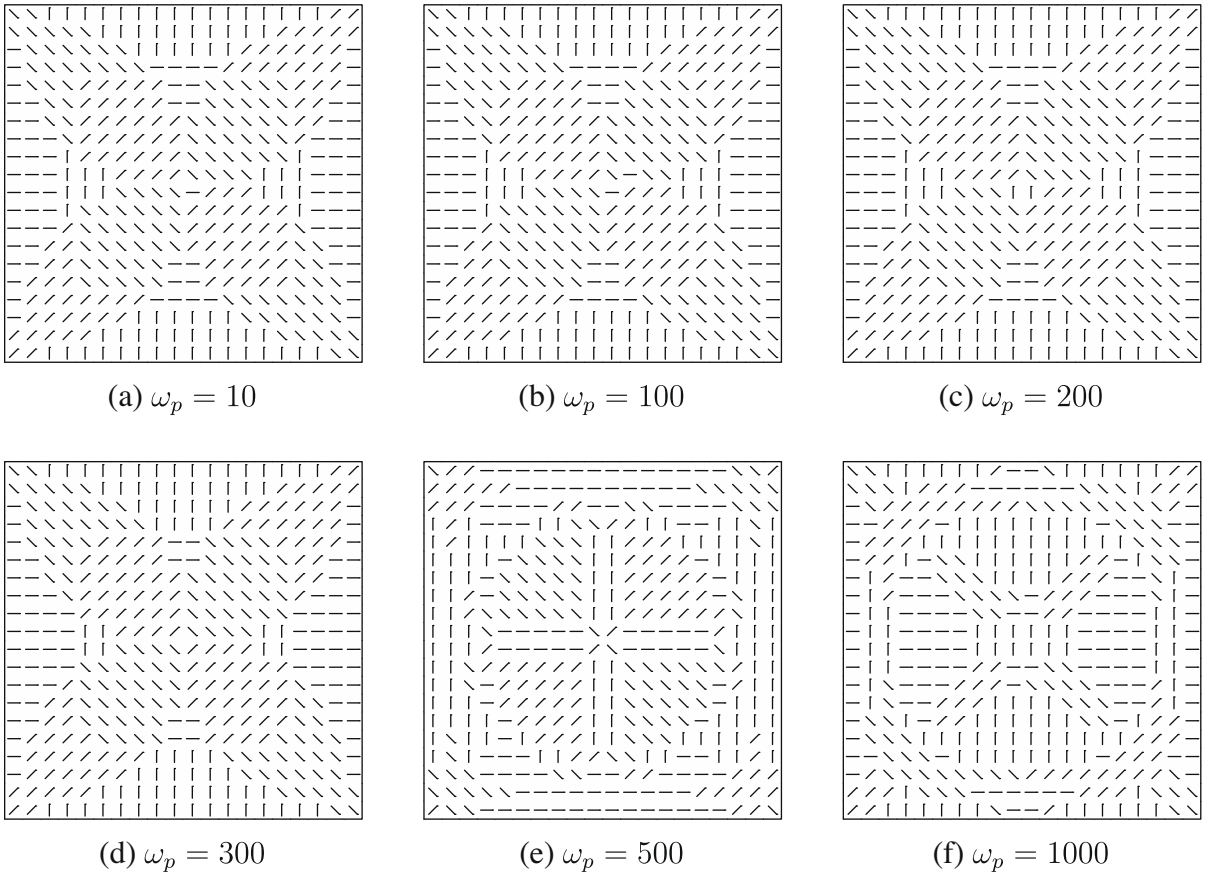

Fig. 5. Single-layer plate: optimized designs for different excitation frequencies.

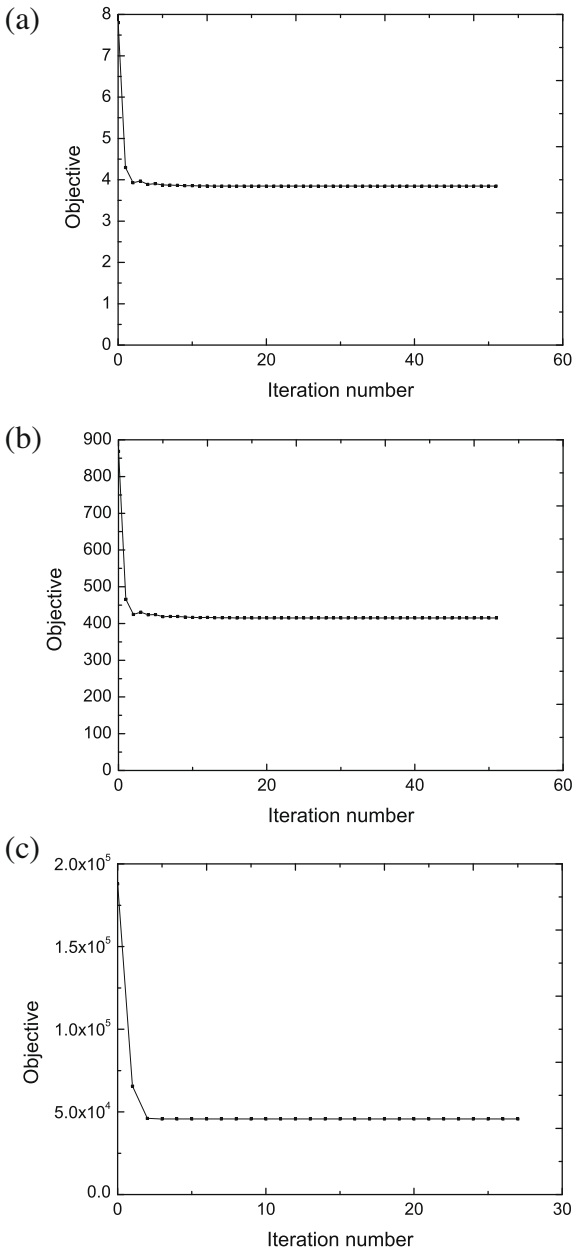

Fig. 6. Iteration histories of the minimum sound radiation designs in Fig. 5(a), (b) and (e): (a) Iteration history for the case of $\omega_p = 10$, (b) for $\omega_p = 100$ and (c) for $\omega_p = 500$.

Table 3
Single-layer plate: comparison of the total sound power radiation from the initial design and the designs optimized for different excitation frequencies ω_p.

Excitation frequency, ω_p	Initial design	Optimized design		Relative decrease
	Sound power, Π_0	Sound power, Π	Fig.	$\lvert\Pi - \Pi_0\rvert/\Pi_0$
10	15.61	7.69	5(a)	50.77%
100	1738	830	5(b)	52.24%
200	10,023	4263	5(c)	57.47%
300	51,001	15,846	5(d)	68.93%
500	375,728	91,434	5(e)	75.66%
1000	9310	7844	5(f)	15.77%

By comparison of results in Tables 1 and 2, we see that the optimization with the excitation frequency prescribed as $\omega_p = 500$ has decreased quite significantly the nearest (first) resonance frequency Ω_1 from the value 434 for the initial design to the value 354 for the optimized design. This implies that large displacement amplitudes have been considerably reduced at the excitation frequency $\omega_p = 500$ by the discrete material optimization, and explains the substantial reduction of the sound radiation by 75.66%. At the same time, the second resonance frequency Ω_2 is slightly decreased by the optimization for the case of $\omega_p = 500$, see Tables 1 and 2, but it is so much larger than the excitation frequency $\omega_p = 500$ that it has only marginally affected the sound power radiation at ω_p.

Hence, for the case of $\omega_p = 500$, the mechanical cause of the substantial reduction of the sound power radiation achieved by the optimization is that the optimization has driven the nearest (first) resonance frequency as far away as possible (i.e., downward) from the prescribed excitation frequency ω_p.

Let us then consider the case of optimization for $\omega_p = 1000$, where the excitation frequency ω_p is roughly located in the middle of the interval between the first and second resonance frequencies $\Omega_1 = 434$ and $\Omega_6 = 1591$ of the initial design, see Table 1. This is generally a favourable location of the excitation frequency for a given design, and is also seen to lead to relatively low sound radiation with a comparatively small difference between the values of the initial and the optimized design (cf. Table 3). With $\omega_p = 1000$, we find that the optimization yields a design (shown in Fig. 5(f)), where the first resonance frequency is decreased from 434 to 398 and the second resonance frequency is increased from 1591 to 1756.

Hence, in this case with $\omega_p = 1000$, the mechanical cause of the reduction of the sound radiation obtained by the optimization (see Table 3) is that both of the neighbouring resonance frequencies have been driven away from the excitation frequency ω_p, and thereby created an enlarged gap between these two resonance frequencies with a reduced level of sound radiation at ω_p and in its vicinity.

6.2. Multi-layer plate

A four-layer laminated plate with equal layer thicknesses and the same uniformly distributed, time-harmonic pressure loading as in Section 6.1 is considered for $\omega_p = 100$, $\omega_p = 500$ and $\omega_p = 1000$. These examples aim to demonstrate that the approach can be also used for multi-layer laminated composite plate structures, see Fig. 4. The geometry and boundary conditions of the plate are the same as in Section 6.1, and the glass/epoxy material with the same moduli of elasticity as in Section 6.1 is used. When a 20×20 mesh discretization is applied, the total number of design variables for this four-layer plate is 6400. The layers are numbered from bottom to top, i.e. layer 4 is the upper layer of the plate.

The optimized plates subject to $\omega_p = 100$, 500 and 1000 are shown in Fig. 7(a)–(c), but only by their upper layer (4) as the fiber angles in general are similar for all layers. The total power flow Π from the optimized plates is reduced from 1738 to 830 for $\omega_p = 100$, from 375,728 to 91,434 for $\omega_p = 500$ and from 9310 to 7844 for $\omega_p = 1000$. Thus, for the given excitation frequencies $\omega_p = 100$, 500 and 1000, the same values of the objective function Π are obtained by optimization of the multi-layer laminated plates considered here and the single-layer plates in Section 6.1 with the same boundary conditions and structural dimensions, cf. the results given in Table 3. For the two higher values of the excitation frequency, $\omega_p = 500$ and $\omega_p = 1000$, the fiber orientations in the layers of each of the optimized multi-layer plates are found to be the same as in the upper layers shown in Fig. 7(b) and (c), respectively, and these fiber orientations correspond precisely to those in the optimized single-layer plates associated with the same excitation frequencies, see Fig. 5(e) and (f). For the lower excitation frequency $\omega_p = 100$, some very few differences can be observed in the

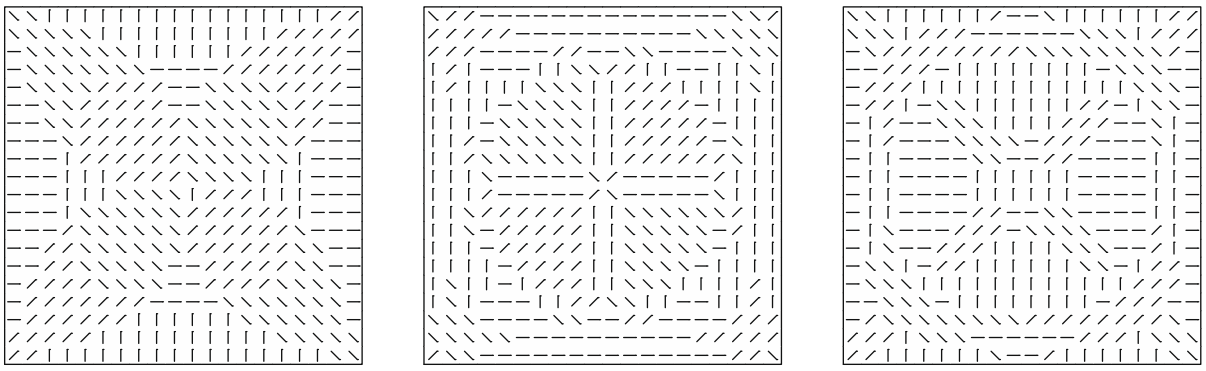

(a) Layer 4, $\omega_p = 100$ (b) Layer 4, $\omega_p = 500$ (c) Layer 4, $\omega_p = 1000$

Fig. 7. Multi-layer plate: optimized designs of the upper layer for different excitation frequencies.

fiber orientations when comparing the upper layer depicted in Fig. 7(a) with the other (non-shown) layers of the optimized multi-layer plate and with the corresponding optimized single-layer plate in Fig. 5(b). These very few differences are found in the narrow central region of the plates where some weighting functions for unidirectional fiber material oriented at [90°, ±45°, 0°] appear to be very close to each other. In agreement with the preceding discussion of the plate designs obtained, the DMO convergence measures (see Section 4) for the optimized multi-layer plate designs with $\omega_p = 100$, 500 and 1000 are found to be $h_{95} = 0.83$, $h_{95} = 0.99$ and $h_{95} = 0.98$, where the value of the convergence measure associated with $\omega_p = 100$ is somewhat smaller than the very high values associated with $\omega_p = 500$ and 1000.

6.3. Laminated sandwich structure

Here and in the following Section 6.4, we consider discrete material optimization for the given excitation frequency $\omega_p = 100$ and 1000 of a laminated structure with the same size and boundary conditions as in the preceding section, but now consisting of eight layers made of glass/epoxy composite and foam material that enable creation of a sandwich structure. The same orthotropic glass/epoxy composite with permissible fiber angles [90°, ±45°, 0°] is used as before, but in addition an isotropic polymeric foam material with Young's modulus $E = 125$ MPa, Poisson's ratio $\nu = 0.3$ and mass density $\gamma = 100$ kg m^{-3} is assumed to be available for the structure.

In this and the subsequent Section 6.4, we choose the given global resource constraint value $\overline{R}$ to represent the total mass of the structural material. Accordingly, we define the unit cost factors u_1 and u_2 (see Section 2) of the unidirectional fiber composite material and the isotropic foam material, respectively, as the mass densities γ_1 and γ_2 of these two materials, and take them to be $u_1 = \gamma_1 = 1900$ and $u_2 = \gamma_2 = 100$ in (8). The allowable total material mass resource constraint value is taken to be $\overline{R} = 10.0$. In view of the data given, this means that the foam must constitute at least 50% of the total volume.

In the current section, we consider the case where the upper and the lower layers are not allowed to choose the polymeric foam, while the inner six layers can locally consist of either the foam or glass/epoxy composite material. This implies 38 design variables per element, distributed as [4, 5, 5, 5, 5, 5, 5, 4] and brings the total number of design variables for the whole plate up to 15200, when a 20×20 finite element mesh is used.

The results of the optimization for $\omega_p = 100$ and 1000 are presented in Figs. 8 and 9, respectively, where layer elements with fibers indicate that the glass/epoxy material is selected with the fiber orientations shown, and elements in white indicate selection of isotropic foam material. The DMO convergence measures for the designs with $\omega_p = 100$ and 1000 are $h_{95} = 0.93$ and $h_{95} = 0.98$, respectively. It is clearly seen from the figures that sandwich-like plates have resulted from both cases of optimization, in particular for the design with $\omega_p = 100$ shown in Fig. 8, where almost all the available foam material is found in the 4 innermost layers (core) of the 8-layer plate. In the design obtained for $\omega_p = 1000$ in Fig. 9, the available foam material is almost entirely placed in the six innermost layers, where it surrounds a short, approximately circular cylinder consisting of the composite material. This will be discussed below. It is also interesting to note that the upper and the lower layer of the optimized designs in both of the two cases considered here, are very similar to the optimized designs of the single-layer plates at the same excitation frequencies, as is seen by comparing the designs of layers 1 and 8 in Figs. 8 and 9 with the design in Fig. 5(b) for $\omega_p = 100$ and the design in Fig. 5(f) for $\omega_p = 1000$, respectively.

As stated in Table 4, we have found that, in comparison with the initial design, the discrete material optimization has reduced the total power flow from 2059 to 967 for $\omega_p = 100$ and from 12,808 to 7969 for $\omega_p = 1000$. Table 4 also lists values of the first and second resonance frequencies Ω_1 and Ω_2 which we, in a similar fashion as described in Section 6.1, have computed for the initial and the two optimized designs in Figs. 8 and 9. These results reveal, like in Section 6.1, that the mechanical explanation for the low values obtained for the sound radiation is that the optimization has either driven the nearest resonance frequency as far away as possible from the prescribed excitation frequency ω_p, or has increased the gap between two neighbouring resonance frequencies as much as possible. Thus, for the design with $\omega_p = 100$ in Fig. 8, the first resonance frequency Ω_1 has been increased quite considerably compared to the first resonance frequency of the initial design, and for the design with $\omega_p = 1000$ in Fig. 9, the gap between the first and second resonance frequencies has been increased by both decreasing the first resonance frequency and increasing the second resonance frequency.

Let us finally discuss the quite remarkable difference between the overall layouts of the inner layers of the optimized plates in Figs. 8 and 9. The plate in Fig. 8 is optimized for an excitation frequency $\omega_p = 100$ that is substantially smaller than the first resonance frequency $\Omega_1 = 666$ of the plate, cf. Table 4. In consistency with minimization of the total sound radiation, the plate may therefore with good approximation be considered to have been subjected to integral static stiffness maximization (i.e., compliance minimization) for a uniformly distributed static loading (corresponding to $\omega_p = 0$) that equals the given amplitude **P** of the

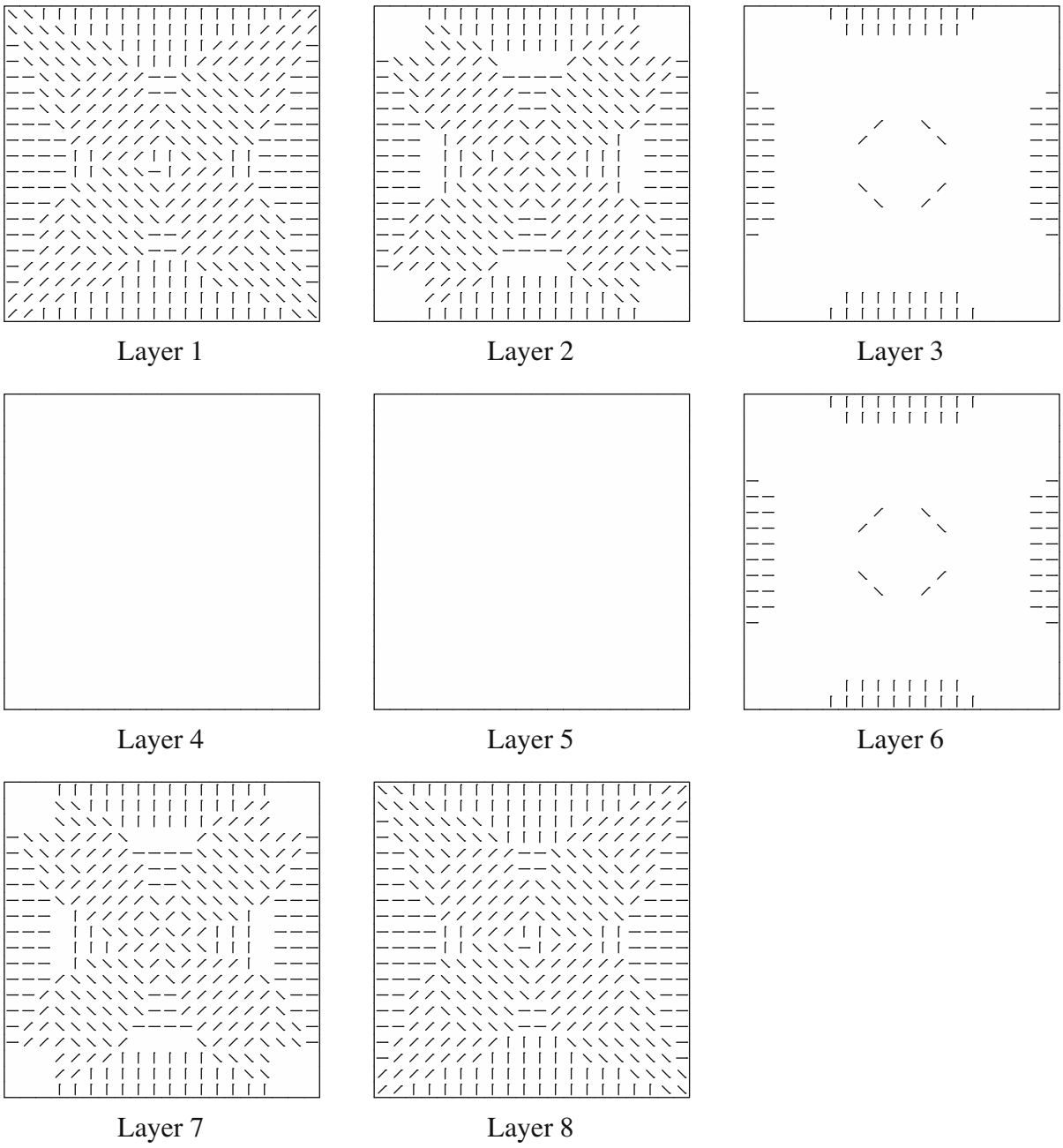

Fig. 8. Sandwich plate: optimized design for the excitation frequency $\omega_p = 100$ when no foam material is allowed in the lower layer 1 and upper layer 8.

(otherwise) harmonic loading. Thus the design should be mainly (bending) stiffness driven. This is confirmed by the design in Fig. 8 where almost all the available stiffer composite material is found in the outermost layers 1,2 and 7,8, while almost all the weaker foam material is found in the inner layers 3–6.

Contrary to Fig. 8, the design in Fig. 9 with $\omega_p = 1000$ has been significantly driven by dynamics, essentially because inertia forces are proportional to the square of the frequency of harmonic vibration of mass. Thus, as is seen, the central part of the plate in Fig. 9 is filled-out by an approximately circular through-the-thickness cylinder consisting of the stiffer composite material that has a much higher mass density than the foam material. This local design of the plate is very efficient in counteracting the time-harmonic external loading that has not only a given frequency ($\omega_p = 1000$) but also a prescribed amplitude, and is found to be in anti-phase with the central part of the forced vibration mode, whose shape is as depicted in Fig. 12(b). Clearly, the mass assembly in the central part of the plate yields a large inertia that very effectively reduces the displacement amplitudes over the central part of the plate, and, thereby, reduces the vibration amplitudes and the density of sound power emission all over the plate.

6.4. Laminated sandwich structure without restriction on the selection of material in the surface layers

Here, we consider the same problem as in the preceding section, but with the exception that the upper and the lower layer are now allowed to choose freely between the polymeric foam and the glass/epoxy composite material like the inner 6 layers. This implies 40 design variables per element, distributed as [5, 5, 5, 5, 5, 5, 5, 5] and bringing the total number of design variables for the whole plate up to 16,000, when a 20×20 finite element mesh is used.

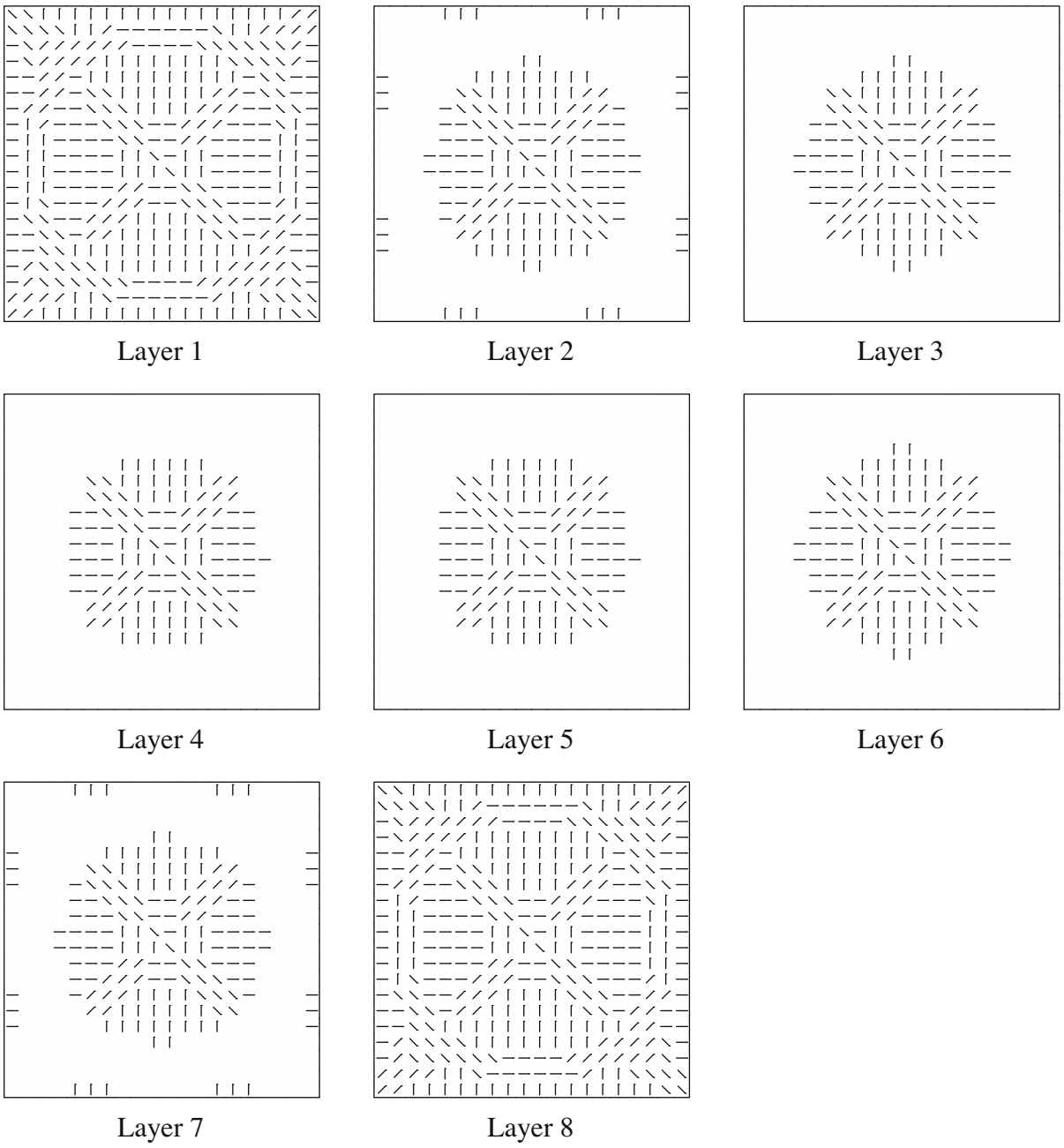

Fig. 9. Sandwich plate: optimized design for the excitation frequency $\omega_p = 1000$ when no foam material is allowed in the lower layer 1 and upper layer 8.

Table 4
Results for the initial and optimized designs of sandwich plates when no foam material is allowed in the surface layers.

	1st resonance freq., Ω_1	2nd resonance freq., Ω_2	Sound radiation for $\omega_p = 100$	Sound radiation for $\omega_p = 1000$
Initial design	449	1656	2059	12,808
Design optimized with $\omega_p = 100$, Fig. 8	666	2114	967	
Design optimized with $\omega_p = 1000$, Fig. 9	369	1984		7969

The plate designs obtained by the discrete material optimization are presented in Fig. 10 with $\omega_p = 100$ and Fig. 11 with $\omega_p = 1000$. The DMO convergence measures for the designs with $\omega_p = 100$ and $\omega_p = 1000$ are $h_{95} = 0.93$ and $h_{95} = 0.98$, respectively, and the resonance frequency and sound radiation characteristics determined for the initial design and the optimized designs in the same way as described earlier, are listed in Table 5. Here it is seen, by comparison with the results given in Table 4 for the optimized designs shown in Figs. 8 and 9, that the total power flow has been slightly reduced from 967 to 952 for the design in Fig. 10 with $\omega_p = 100$, and, more significantly, from 7969 to 6952 for the design in Fig. 11 with $\omega_p = 1000$. Thus, for the same value of the excitation frequency, the designs optimized without restriction on the selection of material in the surface layers in the current section are "more optimal" than those obtained with the restriction in the preceding Section 6.3. This is of course to be expected since the restriction on the selection of material for the surface layers in Section 6.3 implies that the design space is smaller. The mechanical causes of the reductions of the sound radiations from the designs

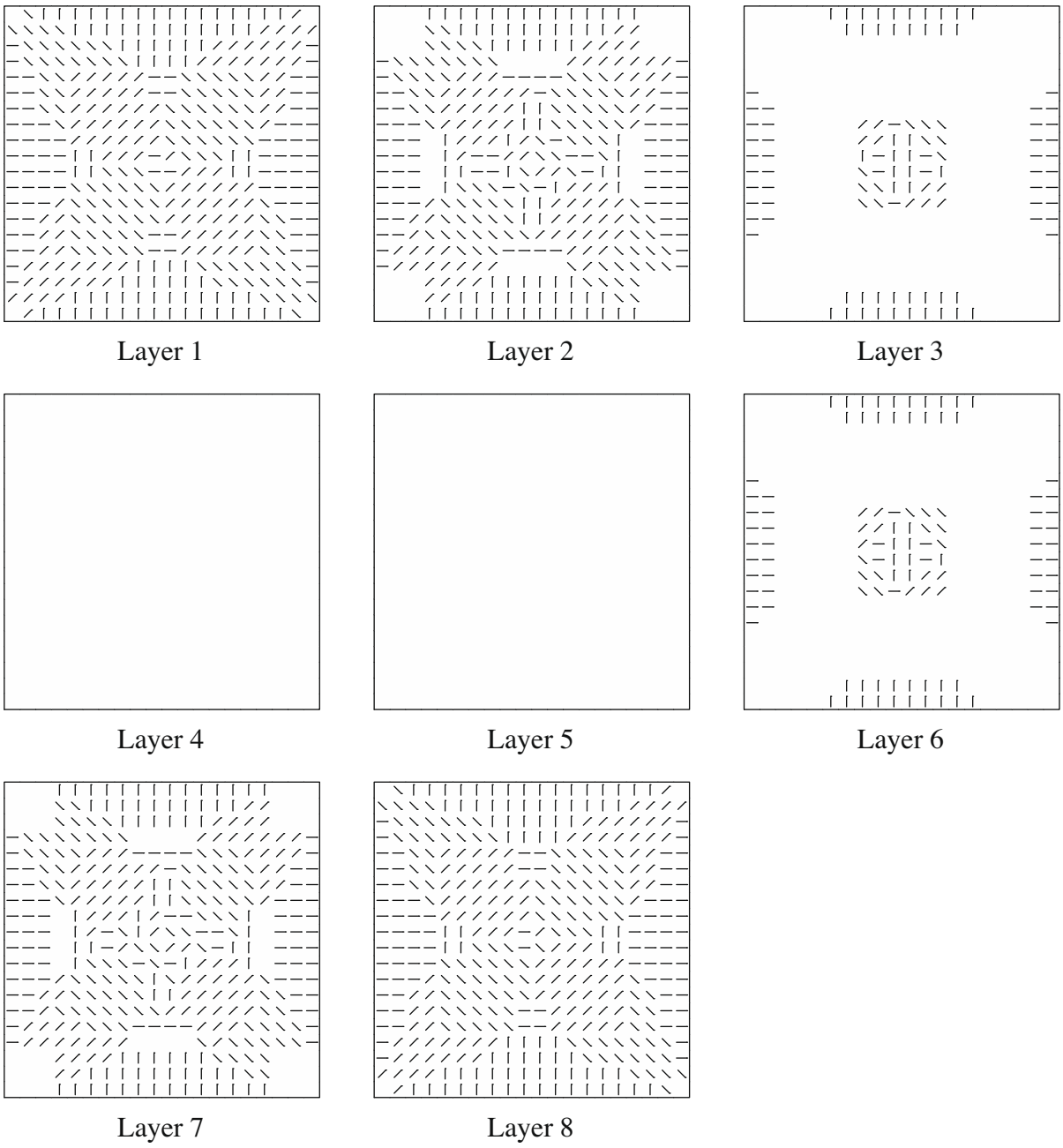

Fig. 10. Sandwich plate: optimized design for the excitation frequency $\omega_p = 100$ and without restriction for the surface layers.

in Figs. 10 and 11 are the same as described for the designs in Figs. 8 and 9, respectively, in Section 6.3.

By comparing the optimized designs in Figs. 10 and 11 with the corresponding ones in Figs. 8 and 9, respectively, it appears that the removal of the restriction against use of foam material in the surface layers has only given rise to minor changes in the surface layers. This is particularly the case for the design in Fig. 10 with $\omega_p = 100$, where the surface layers 1 and 8 consist of composite material except for very small regions with foam material in the corners. The inner layers of this design also only exhibit very small changes. The forced vibration mode of the optimized design in Fig. 10 excited at $\omega_p = 100$ has the same phase as the uniformly distributed dynamic loading, and is shown in Fig. 12(a).

The surface layers of the design optimized with $\omega_p = 1000$ in Fig. 11 also predominantly consist of composite material, and the inner layers of the plate are seen to exhibit only minor changes relative to the corresponding layers in Fig. 9. However, it is noteworthy that in the surface layers of the plate in Fig. 11, a thin, ring-like shaped region consisting of foam material is found between the large central part of each of the surface layers and the edges of the plate. Moreover, a close inspection of all the layers of the plate in Fig. 11 reveals that (with some small, unimportant exceptions in the innermost layers 4 and 5), the entire plate is equipped with an inner, through-the thickness zone of foam material that emanates from the thin, ring-shaped regions with foam in the surface layers, and follows these regions all the way around the large central part of the plate. A mechanical explanation of this feature of the plate design in Fig. 11, which is optimized for and excited by $\omega_p = 1000$, may be given by considering the corresponding forced vibration mode in Fig. 12(b), where the outer part of the plate along the clamped edges is found to be in-phase, and the central part of the plate to be in anti-phase with the uniformly distributed

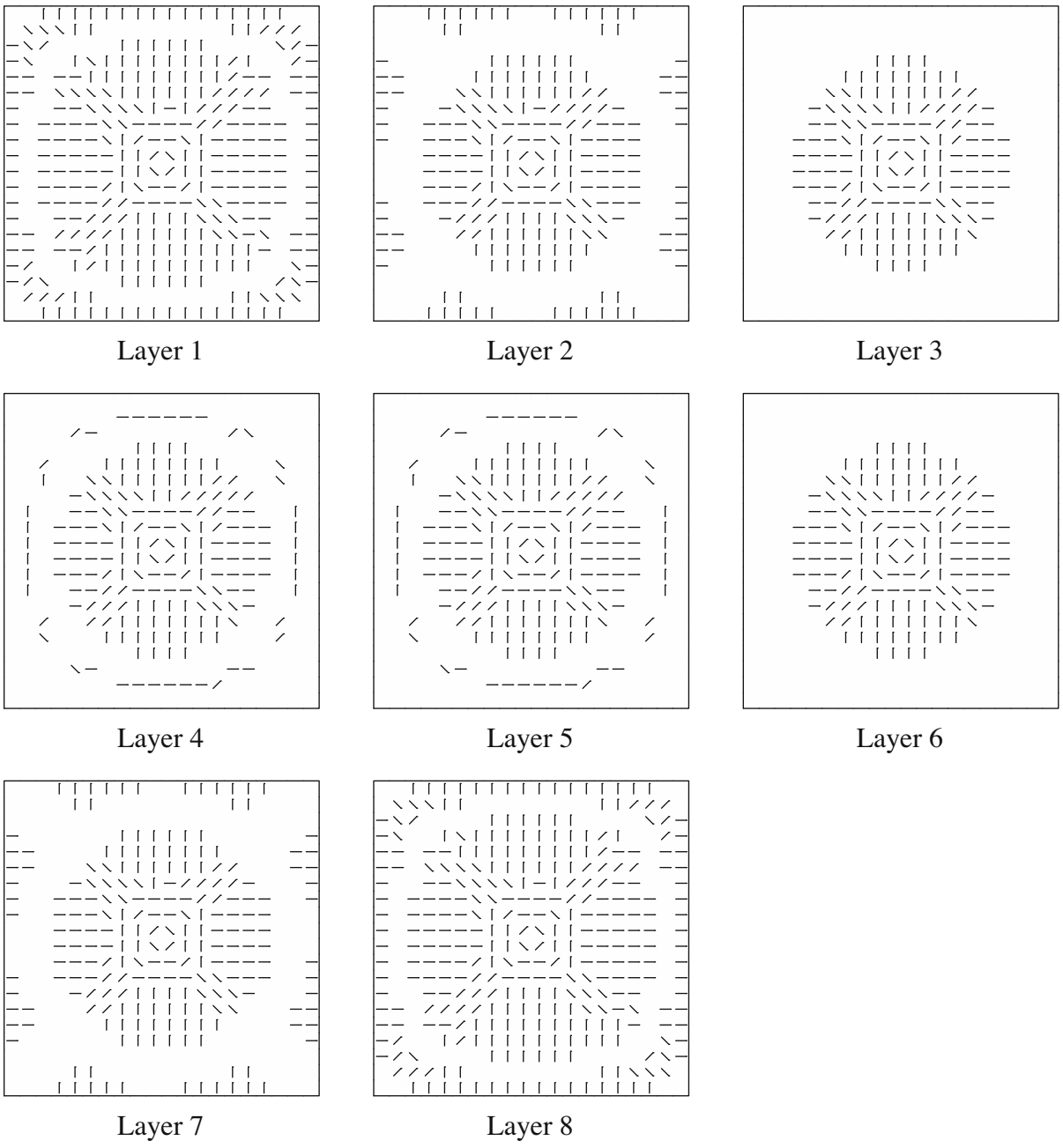

Fig. 11. Sandwich plate: optimized design for the excitation frequency $\omega_p = 1000$ and without restriction for the surface layers.

Table 5
Results for the initial and optimized designs of sandwich plates without restriction for the surface layers.

	1st resonance freq., Ω_1	2nd resonance freq., Ω_2	Sound radiation for $\omega_p = 100$	Sound radiation for $\omega_p = 1000$
Initial design	432	1594	2713	14,152
Design optimized with $\omega_p = 100$, Fig. 10	623	2029	952	
Design optimized with $\omega_p = 1000$, Fig. 11	281	1963		6952

harmonic dynamic loading. Guided by Fig. 12(b), we have found that within the thin, ring-like plate region with foam material in the surface layers, there exists a closed curve along which the two principal bending curvatures are zero and very small, respectively. This means that from the point of view of optimization, the through-the-thickness application of the isotropic, low-stiffness foam material is "optimal" in this region of the plate, and that it saves composite material here for other regions where high stiffnesses are useful.

7. Discussion of the DMO of a single-layer plate with unidirectional fibers and two isotropic materials

The DMO parameterization used in this paper enforces unit value of the sum of the weighting functions, see (9), which is important for a physical interpretation of the designs and for correct evaluation of quantities such as the mass, weight and cost, etc. For example, a design having the sum of the weighting functions

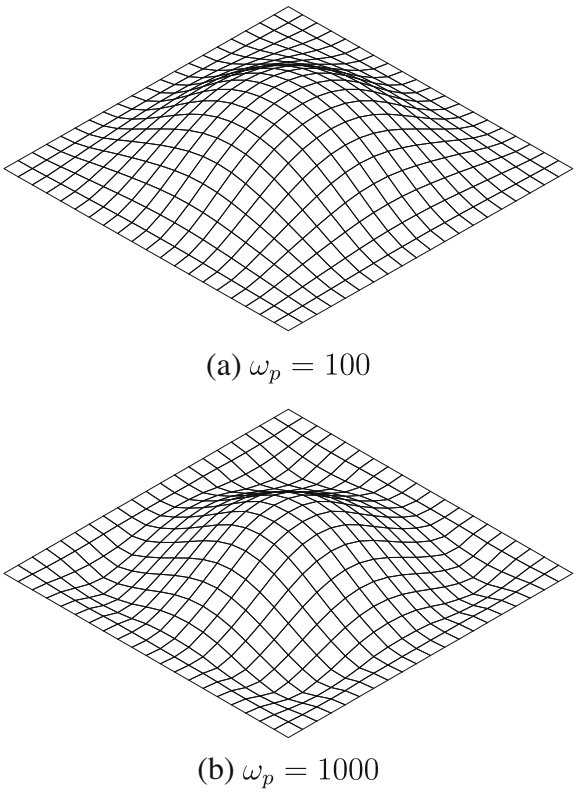

Fig. 12. Forced vibration modes of the plate designs (a) optimized for and excited at $\omega_p = 100$ in Fig. 10, and (b) optimized for and excited at $\omega_p = 1000$ in Fig. 11.

greater than one in the optimization process is not meaningful from a physical point of view because more than one material would then be selected for the same element. According to the studies of Stegmann and Lund (2005), Stegmann (2004) and Hvejsel and Lund (2009), the penalization scheme with the unity constraint alters the effect of penalizing the design variables compared to the similar penalization scheme without the unity constraint. Thus, in some cases, it is less effective in driving all the design variables to their limits.

In this paper, this behavior has been observed in some plate sub-regions in which two candidate materials performed equally well or where the available candidate materials may not have included a more optimal material. Thus, in some of the examples in Section 6 with excitation frequencies lower than the first resonance frequencies of the optimized plates, the distribution of fiber orientations is not found to be completely symmetric in the central area because the optimization has not completely converged due to the drawback of the interpolation function. The reason for this may have been that an optimum choice of material has not been possible from among the set of available candidate materials considered. As an example, see Thomsen and Olhoff (1990), for the different problem of a flat plate subjected to in-plane loading that caused in-plane shear-dominated sub-regions, it was necessary to allow for orthogonal cross-ply fiber arrangements rather than just unidirectional fibers in order to achieve convergence of the optimum design.

For the problem of a single-layer plate as considered in Section 6.1, in-plane shear is negligible. However, if we consider the plate design optimized for $\omega_p = 100$ in Fig. 5(b), there are some layer elements where the weighting functions associated with the fiber orientations of ±45°, 90° and 0° of the given candidate materials are very close to each other, and where deviations from symmetry occur. To study this unwanted behaviour, we first extend the set of candidate materials by choosing the enlarged set of fiber angles [90°, ±75°, ±60°, ±45°, ±30°, ±15°, 0°] of the same unidirectional composite with material properties as considered in Section 6.1 (also listed as material #1 in Table 6), and solve the otherwise self-same problem as in Fig. 5(b) with $\omega_p = 100$. The optimized design resulting from this extension of the set of available fiber angles from 4 to 12 is illustrated in Fig. 13.

By comparing the design optimized for $\omega_p = 100$ in Fig. 13 with the corresponding one in Fig. 5(b), the total power flow has been reduced from 830 to 789 as is to be expected in view of the extension of the design space. However, the increase of the set of available fiber angles from 4 to 12 in each element of the plate has not removed or reduced the occurrence of a minor number of deviations from symmetry in the distribution of fiber orientations in the plate, and in comparison with the DMO convergence measure $h_{95} = 0.82$ determined for the design in Fig. 5(b), it is found that this measure is only $h_{95} = 0.75$ for the design in Fig. 13.

Now, by considering the plate design in Fig. 13 and the corresponding forced vibration mode which at the excitation frequency $\omega_p = 100$ is very similar to that depicted in Fig. 12(a), it is reasonable to assume that the rotational symmetry indicated in the central part of both the design and the vibration mode reflects a state with equal principal bending moments in the region around the mid-point of the plate. Moreover, it is well-known from various studies of optimization of elastic as well as perfectly plastic plates with respect to different design objectives that the optimum solution in such a region is a solid, isotropic plate design, see e.g., Cheng (1981), Cheng and Olhoff (1982), Rozvany et al. (1982), Wang et al. (1984).

Along these lines, together with the unidirectional composite termed "material #1" in Table 6 and to be considered again with the fiber angles [90°, ±75°, ±60°, ±45°, ±30°, ±15°, 0°], we shall now include first a weaker and then also a stiffer isotropic elastic material, which in Table 6 are called "material #2" and "material #3", respectively, as candidate materials in the DMO of the single-layer plate for $\omega_p = 100$.

Table 6
Elastic properties, mass densities γ_i and unit monetary cost factors c_i for a unidirectional fiber material and two isotropic materials.

Material #1 (unidirectional fiber composite)	Material #2 (isotropic)	Material #3 (isotropic)
$E_x = 54$ GPa	$E = 8$ GPa	$E = 25$ GPa
$E_y = 18$ GPa		
$E_z = 18$ GPa		
$G_{xy} = G_{yz} = G_{zx} = 9$ GPa		
$\upsilon_{xy} = 0.25$	$\nu = 0.3$	$\nu = 0.3$
$\gamma_1 = 1900$ kg m^{-3}	$\gamma_2 = 1000$ kg m^{-3}	$\gamma_3 = 1000$ kg m^{-3}
$c_1 = 1500$ m^{-3}	$c_2 = 100$ m^{-3}	$c_3 = 1000$ m^{-3}

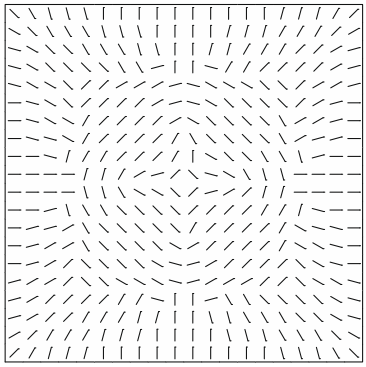

Fig. 13. Optimized design for minimum sound radiation at $\omega_p = 100$ from single-layer clamped quadratic plate made of unidirectional fiber material with 12 available fiber angles [90°, ±75°, ±60°, ±45°, ±30°, ±15°, 0°].

To accommodate the introduction of both isotropic and unidirectional fiber materials as candidate materials in the DMO, we in this chapter consider a total (monetary) cost constrained problem, where the unit cost factors u_1, u_2 and u_3 (see Chapter 2) represent the monetary unit cost factors c_1, c_2 and c_3 for the unidirectional and the two isotropic materials. Thus, in (8) we set $u_1 = c_1 = 1500$ for material #1, $u_2 = c_2 = 100$ for material #2, and $u_3 = c_3 = 1000$ for material #3, cf. Table 6, where we have omitted to state the specific currency. The allowable total cost constraint value is chosen to be $\overline{R} = 6.0$. This value may be compared with the value $\overline{R} = 15$ of the total cost of the optimized design in Fig. 13 where the entire plate is made of composite material (whose fiber angles do not affect the value of $\overline{R}$).

If we start out optimizing the single-layer clamped quadratic plate by DMO for $\omega_p = 100$ and $\overline{R} = 6.0$ with candidate materials that include the unidirectional material (#1) with the different fiber angles [90°, ±75°, ±60°, ±45°, ±30°, ±15°, 0°] and only the isotropic material (#2) with the low Young's modulus $E = 8$ GPa, cf. Table 6, we get the design illustrated in Fig. 14(a). Here, elements with fibers indicate that the unidirectional fiber material (#1) is selected with the fiber orientations shown, and elements in white indicate selection of the weaker isotropic material (#2). It is observed in Fig. 14(a) that the stiffer unidirectional fiber material is distributed along the mid-parts of the clamped edges and in a star-shaped mid-region of the plate, while the much weaker isotropic material (#2) is distributed in the remainder of the plate. It is apparent that the stiffness of the isotropic material (#2) has been too low to ensure placement of part of this material in the central region of the plate, and it is seen that there are a few deviations from symmetry in the distribution of the fiber orientations near the mid-point of the plate. The DMO convergence measure is found to be $h_{95} = 0.88$ for the optimized design in Fig. 14(a), and the total sound power radiation from the plate at $\omega_p = 100$ is determined to be 1655.

Following the discussion above, we shall now solve the same problem as the preceding one of optimizing the single-layer clamped quadratic plate for $\omega_p = 100$ and $\overline{R} = 6.0$, however with the exception that now we also include the isotropic material #3 among the available candidate materials for the DMO. In Table 6, the Young's modulus of this isotropic material is seen to be about three times that of the weaker isotropic material #2, and about 1.4 and 0.46 times the Young's moduli in the transverse and longitudinal fiber directions, respectively, of the composite material (#1) which represents a unidirectional glass/epoxy composite. The unit cost factor of the new, stiffer isotropic material (#3) is 10 times that of the weaker isotropic material (#2) and two thirds of the cost factor of the composite material (#1), see Table 6. It should be mentioned that the optimum design is very much dependent on the elastic properties of the materials, the unit costs of these materials, and the given upper bound value $\overline{R}$ on the resource.

The optimum design of the plate associated with the data given in Table 6 is presented in Fig. 14(b), where elements in grey indicate selection of the stronger isotropic material (#3). It is observed that, as conjectured, the stronger isotropic material (#3) is found and distributed in the central region of the plate instead of unidirectional fiber material (#1), and it is interesting to note that the former is partly surrounded by smaller regions of the latter. It is also noteworthy that the design in Fig. 14(b) is found to be perfectly symmetric, and the DMO convergence measure is $h_{95} = 0.97$. The total sound power radiation from the optimized design at $\omega_p = 100$ in Fig. 14(b) is found to be 1567, which is clearly smaller, and hence "more optimal" than the value 1655 of the sound power radiation from the design in Fig. 14(a), given that the two designs are associated with the same total cost, $\overline{R} = 6.0$.

All in all the investigation in this section indicates that the inclusion of the stiffer isotropic material in the set of candidate materials for the DMO problem considered has provided a pertinent regularization of the problem. A similar regularization may prove to be useful for some of the other problems with a low value of the excitation frequency ω_p considered in Section 6.

Finally, it is very interesting to compare the optimum plate design in Fig. 14(b) with a thickness distribution, see Fig. 15, obtained numerically by Cheng and Olhoff (1981) for the problem of maximizing the integral stiffness (minimizing the compliance) of a clamped, quadratic elastic plate of given material volume and plate domain, for which a minimum and a maximum constraint are

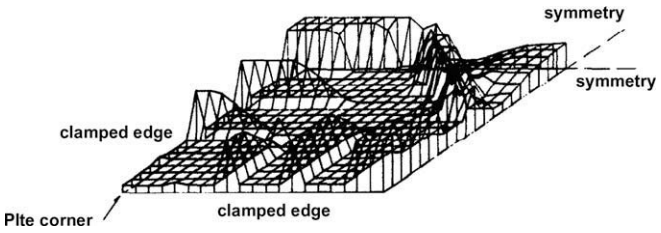

Fig. 15. Optimized design of quarter of a clamped square plate for maximum integral stiffness (Cheng and Olhoff, 1981).

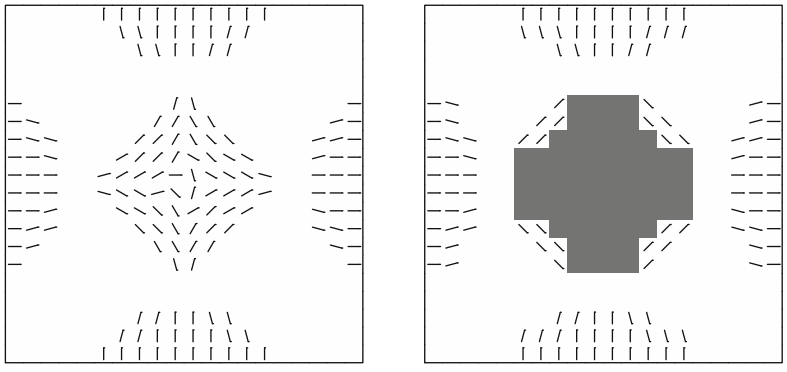

Fig. 14. Optimized designs for minimum sound radiation at $\omega_p = 100$ from single-layer clamped quadratic plate with unidirectional fiber and isotropic materials of total cost $\overline{R} = 6.0$. The unidirectional fiber material has 12 available fiber angles [90°, ±75°, ±60°, ±45°, ±30°, ±15°, 0°]: (a) unidirectional fiber material (#1) and isotropic material (#2), total sound radiation is 1655, (b) unidirectional fiber material (#1) and isotropic materials (#2) and (#3) (cf. Table 6), with smaller total sound radiation, 1567.

specified for the variable plate thickness. Actually, following preceding work by Olhoff (1975, 1981) and Cheng (1981), the objective of the paper by Cheng and Olhoff (1981) was to study the formation of plate ribs (or stiffeners), and it led to the development of a new formulation for plate optimization problems, see Cheng and Olhoff (1982), that may be considered a forerunner for the development of the more general method of topology optimization as it is known today.

Now, by comparing the layout of the fibers and of the regions with the isotropic materials with lower and higher stiffnesses, respectively, in the optimum plate design in Fig. 14(b), this layout is seen to be remarkably similar to the layout in Fig. 15 of the ribs, the region with active minimum plate thickness constraint, and the mid-region of the plate where the thickness is varying smoothly between inactive constraints.

As was pointed out by Profs. Prager and Rozvany, see Rozvany et al. (1995), the layout of the ribs in Fig. 15, and hence of the fibers in Fig. 14(b), is also remarkably similar to results obtained by Rozvany and Adidam (1972) and Prager (1977a,b) for a quite different problem, namely optimum layout of grillages in minimum weight design of rectangular grillage structures against plastic collapse.

8. Conclusions

Minimum sound radiation from vibrating laminated composite plates without damping is considered in this paper. The plates are subjected to uniformly distributed time-harmonic pressure loading with prescribed frequency and amplitude. Since the plate surfaces are flat, instead of solving the Helmholtz equation, Rayleigh's approximation is used for computing the total sound power radiated from the plate into a light acoustic medium such as air. This substantially reduces the computational cost of the structural–acoustic analysis and design optimization. Optimization of fiber orientations, stacking sequence and material selection is performed by Discrete Material Optimization (DMO) for quadratic, clamped single-layer, multi-layer and sandwich plates. Interesting features of the optimized designs are observed in numerical examples.

Numerical results for single-layer and multi-layer plates show that the fiber orientations of the layers in each of the optimized multi-layer plates are generally found to be the same and to correspond to those in the optimized design of the corresponding single-layer plate at the same excitation frequency. In the design of laminated plates with polymeric foam and glass/epoxy composite material as candidate materials, sandwich-like plates have been obtained for the excitation frequencies considered. The influence of a restriction on the selection of candidate materials for the surface layers on the optimum topologies is discussed. For the same type of plate structure and excitation frequency, the design optimized without restriction on candidate materials for the surface layers is consistently better than the design optimized subject to the restriction.

The total sound power radiation from the vibrating laminated composite plates is generally significantly decreased by the discrete material optimization. To minimize the sound radiation, the optimization has either driven the nearest resonance frequency as far away as possible from the prescribed excitation frequency, or has increased the gap between two neighbouring resonance frequencies as much as possible. For an excitation frequency smaller than the first resonance frequency, the design is mainly (bending) stiffness driven, while the design is driven by dynamics for higher values of the excitation frequency, and this furnishes quite remarkable differences in the optimized designs.

In the end of the paper, a cost constrained single-layer plate problem with a low excitation frequency is considered in order to investigate the introduction of two isotropic materials in addition to unidirectional fiber materials as candidate materials in the DMO. It is found that the stiffer of the two isotropic materials is distributed in the central region of the plate instead of unidirectional fiber material, which is then mainly distributed along the mid-parts of the clamped edges of the plate, while the weaker isotropic material is distributed in the remainder of the plate. Remarkably similar layouts have been obtained earlier for quite different optimization problems for elastic and perfectly plastic structures.

There is still a need to further investigate weighting functions in the DMO approach for the general case with a large number of candidate materials in order to both fulfil the unity demand and penalize intermediate densities more effectively. Furthermore, optimization with respect to a band of excitation frequencies taking the structural damping into account may be considered in future work.

Acknowledgements

This work was partially supported by the National Natural Science Foundation of China (Grant No. 90816025), the Danish Center for Applied Mathematics and Mechanics (DCAMM), and Aalborg University. This support is gratefully acknowledged by the authors.

References

Akl, W., El-Sabbagh, A., Al-Mitani, K., Baz, A., 2009. Topology optimization of a plate coupled with acoustic cavity. Int. J Solids Struct. 46, 2060–2074.
Bendsøe, M.P., Olhoff, N., 1985. A method of design against vibration resonance of beams and shafts. Optim. Control Appl. Meth. 6, 191–200.
Bendsøe, M.P., Kikuchi, N., 1988. Generating optimal topologies in structural design using a homogenization method. Comput. Meth. Appl. Mech. Eng. 71, 197–224.
Bendsøe, M.P., Diaz, A.R., 1994. Optimization of material properties for improved frequency response. Struct. Optim. 7, 138–140.
Bendsøe, M.P., Sigmund, O., 2003. Topology Optimization: Theory, Methods and Applications. Springer, Berlin.
Bendsøe, M.P., Lund, E., Olhoff, N., Sigmund, O., 2005. Topology optimization – broadening the areas of application. Control Cybernet. 34, 7–35.
Bendsøe, M.P., Olhoff, N., Sigmund, O. (Eds.), 2006. Proc. IUTAM Symp. Topological Design Optimization of Structures, Machines and Materials – Status and Perspectives, Copenhagen, Denmark, October 26–29. Springer, Berlin, 2005.
Bös, J., 2006. Numerical optimization of the thickness distribution of three-dimensional structures with respect to their structural acoustic properties. Struct. Optim. 32, 12–30.
Calvel, S., Mongeau, M., 2005. Topology optimization of a mechanical component subject to dynamic constraints. Technical Report LAAS N^0 05374. Available from: <http://mip.ups-tlse.fr/perso/mongeau>.
Chen, S.H., Song, X.W., Yang, Z.J., 2005. Modal optimal control of cabin noise of vehicles. Smart Mater. Struct. 14, 257–264.
Cheng, G., 1981. On non-smoothness in optimal design of solid elastic plates. Int. J. Solids Struct. 17, 795–810.
Cheng, G., Olhoff, N., 1981. An investigation concerning optimal design of solid elastic plates. Int. J. Solids Struct. 17, 305–323.
Cheng, G., Pedersen, P., 1997. On sufficiency conditions for optimal design based on extremum principles of mechanics. J. Mech. Phys. Solids 45, 135–150.
Cheng, G., Olhoff, N., 1982. Regularized formulation for optimal design of axisymmetric plates. Int. J. Solids Struct. 18, 153–169.
Christensen, S.T., Sorokin, S.V., Olhoff, N., 1998a. On analysis and optimization in structural acoustics – part I: problem formulation and solution techniques. Struct. Optim. 16, 83–95.
Christensen, S.T., Sorokin, S.V., Olhoff, N., 1998b. On analysis and optimization in structural acoustics – part II: exemplifications for axisymmetric structures. Struct. Optim. 16, 96–107.
Denli, H., Sun, J.Q., 2007. Structural-acoustic optimization of composite sandwich structures: a review. Shock Vib. Dig. 39 (3), 189–200.
Dias, A.R., Kikuchi, N., 1992. Solutions to shape and topology eigenvalue optimization problems using a homogenization method. Int. J. Numer. Mech. Eng. 25, 1487–1502.
Diaz, A.R., Haddow, A.G., Ma, L., 2005. Design of band-gap grid structures. Struct. Multidiscip. Optim. 29 (6), 418–431.
Du, J., Olhoff, N., 2007a. Minimization of sound radiation from vibrating bi-material structures using topology optimization. Struct. Multidiscip. Optim. 33, 305–321.
Du, J., Olhoff, N., 2007b. Topological design of freely vibrating continuum structures for maximum values of simple and multiple eigenfrequencies and frequency gaps. Struct. Multidiscip. Optim. 34, 91–110.
Du, J., Olhoff, N., 2010. Topological design of vibrating structures with respect to optimum sound pressure characteristics in a surrounding acoustic medium. Struct. Multidiscip. Optim. (published online), doi:10.1007/s00158-009-0477-y.

Dühring, M.B., Jensen, J.S., Sigmund, O., 2008. Acoustic design by topology optimization. J. Sound Vib. 317, 557–575.
Eschenauer, H., Olhoff, N., 2001. Topology optimization of continuum structures: a review. Appl. Mech. Rev. 54, 331–389.
Foldager, J., Hansen, J.S., Olhoff, N., 1998. A general approach forcing convexity of ply angle optimization in composite laminates. Struct. Optim. 16, 201–211.
Halkjær, S., Sigmund, O., Jensen, J.S., 2006. Maximizing band gaps in plate structures. Struct. Multidiscip. Optim. 32, 263–275.
Herrin, D.W., Martinus, F., Wu, T.W., Seybert, A.F., 2003. A New Look at the High Frequency Boundary Element and Rayleigh Integral Approximations. Society of Automotive Engineers, Warrendale, PA.
Hufenbach, W., Kroll, L., Holste, C., Täger, O., Barkanov, E., 2001. Design of dynamically loaded fiber-reinforced structures with account of their vibro-acoustic behavior. Mech. Compos. Mater. 37 (2), 145–152.
Hvejsel, C.G., Lund, E., 2009. Interpolation schemes in discrete material optimization. In: Proc. of the 8th World Congress of Structural and Multidisciplinary Optimization, Lisbon, Portugal, June 2009.
Jensen, J.S., 2003. Phononic band gaps and vibrations in one- and two-dimensional mass-spring structures. J. Sound Vib. 266, 1053–1078.
Jensen, J.S., Pedersen, N.L., 2006. On maximal eigenfrequency separation in two-material structures: the 1D and 2D scalar cases. J. Sound Vib. 289, 967–986.
Jensen, J.S., 2007. Topology optimization of dynamic problems with Padé approximants. Int. J. Numer. Meth. Eng. 72, 1605–1630.
Jensen, J.S., 2009. Space-time topology optimization for one-dimensional wave propagation. Comput. Meth. Appl. Mech. Eng. 198, 705–715.
Jog, C.S., 2002a. Topology design of structures subjected to periodic loading. J. Sound Vib. 253 (3), 687–709.
Jog, C.S., 2002b. Reducing radiated sound power by minimizing the dynamic compliance. In: Munjal, M.L. (Ed.), Proc. of the IUTAM Symp. Designing for Quietness, Bangalore, India, December 12–14, 2000. Kluwer Academic Publishers, Dordrecht, The Netherlands, 19 pp.
Kollmann, F.G., 2000. Machine Acoustics – Basics Measurement Techniques Computation Control, second rev. ed. Springer, Berlin (in German).
Koopmann, G.H., Fahnline, J.B., 1997. Designing Quiet Structures: A Sound Power Minimization Approach. Academic Publishers, London.
Kosaka, I., Swan, C.C., 1999. A symmetry reduction method for continuum structural topology optimization. Comput. Struct. 70, 47–61.
Krog, L.A., Olhoff, N., 1999. Optimum topology and reinforcement design of disk and plate structures with multiple stiffness and eigenfrequency objectives. Comput. Struct. 72, 535–563.
Lax, M., Feshbach, H., 1947. On the radiation problem at high frequencies. J. Acoust. Soc. Am. 19, 682–690.
Lund, E., 1994. Finite element based design sensitivity analysis and optimization. Ph.D. Thesis, Special Report No. 23, Dept. of Mechanical Engineering, Aalborg University, Denmark.
Lund, E., 2009. Buckling topology optimization of laminated multi-material composite shell structures. Compos. Struct. 91, 158–167.
Lund, E., Stegmann, J., 2005. On structural optimization of composite shell structures using a discrete constitutive parametrization. Wind Energy 8, 109–124.
Luo, J.H., Gea, H.C., 1998. Optimal bead orientation of 3D shell/plate structures. Finite Elem. Anal. Des. 31, 55–71.
Luo, J., Gea, H.C., 2003. Optimal stiffener design for interior sound reduction using a topology optimization based approach. J. Vib. Acoust. 125, 267–273.
Ma, Z.D., Kikuchi, N., Cheng, H.C., 1995. Topological design for vibrating structures. Comput. Meth. Appl. Mech. Eng. 121, 259–280.
Mackerle, J., 2003. Topology and shape optimization of structures using FEM and BEM – a bibliography (1999–2001). Finite Elem. Anal. Des. 39, 243–253.
Mendonca, F.H., Neves, M.M., Lau, F.J.P., Gerges, S.N.Y., Bento Coelho, J.L., 2009. On the effect of undamped frequency maximization for the turbulent flow-induced vibrations of a viscoelastically supported plate. In: Proc. of the 8th World Congress of Structural and Multidisciplinary Optimization, Lisbon, Portugal, June 2009.
Miki, M., Sugiyama, Y., 1993. Optimum design of laminated composite plates using lamination parameters. AIAA J. 31, 921–922.
Min, S., Kikuchi, N., Park, Y.C., Kim, S., Chang, S., 1999. Optimal topology design of structures under dynamic loads. Struct. Optim. 17, 208–218.
Mroz, Z., Rozvany, G.I.N., 1975. Optimal design of structures with variable support conditions. J. Optim. Theory Appl. 15, 85–101.
Munjal, M.L. (Ed.), 2002. Proc. of the IUTAM Symp. Designing for Quietness, Bangalore, India, December 12–14. Kluwer Academic Publishers, Dordrecht, The Netherlands, 2000.
Niordson F., Olhoff N., 1979. Variational methods in optimization of structures. In: Besseling, J.F., van der Heijden, A.M.A. (Eds.), Proc. of the W.T. Koiter Anniversary Symp. on Trends in Solid Mechanics, Sijthoff & Nordhoff, 1979, pp. 177–194.
Olhoff, N., 1975. On singularities, local optima and formation of stiffeners in optimal design of plates. In: Sawczuk, A, Mroz, Z (Eds.), Proc. of the IUTAM Symp. on Optimization in Structural Design, Warsaw, Springer, Berlin, 1973, pp. 82–103.
Olhoff, N., Taylor, J.E., 1978. Designing continuous columns for minimum total cost of material and interior supports. J. Struct. Mech. 6, 367–382.
Olhoff, N., Taylor, J.E., 1979. Optimal structural remodeling. J. Optim. Theory Appl. 27, 571–582.
Olhoff, N., Lurie, K.A., Cherkaev, A.V., Fedorov, A.V., 1981. Sliding regimes and anisotropy in optimal-design of vibrating axisymmetric plates. Int. J. Solids Struct. 17, 931–948.
Olhoff, N., Parbery, R., 1984. Designing vibrating beams and rotating shafts for maximum difference between adjacent natural frequencies. Int. J. Solids Struct. 20, 63–75.
Olhoff, N., Du, J., 2005. Topology optimization of structures against vibration and noise. In: Bento Coelho, J.L., Alarcao, D. (Eds.), Proc. of the 12th International Congress on Sound and Vibration, ICSV12, Lisbon, Portugal, July 11–14, 2005, 20 pp.
Olhoff, N., Du, J., 2008. On topological design optimization of structures against vibration and noise emission. In: Sandberg, G., Ohayon, R. (Eds.), Computational Aspects of Structural Acoustics and Vibrations, ISBN 978-3-211-89650-1, Springer Series: CISM International Centre for Mechanical Sciences, Springer, Berlin, 2008, pp. 217–276.
Olhoff, N., Du, J., 2010. Topological design for minimum dynamic compliance of continuum structures subjected to forced vibration. Struct. Multidiscip. Optim., accepted for publication.
Pedersen, N.L., 2000. Maximization of eigenvalues using topology optimization. Struct. Multidiscip. Optim. 20, 2–11.
Pedersen, P., 1982. Design with several eigenvalue constraints by finite elements and linear programming. J. Struct. Mech. 10, 243–371.
Pedersen, P., 1989. On optimal orientation of orthotropic materials. Struct. Optim. 1, 101–106.
Pedersen, P., 1991. On thickness and orientational design with orthotropic materials. Struct. Optim. 3, 69–78.
Prager, W., 1977a. Optimal layout of cantilever trusses. J. Optim. Theory Appl. 23, 111–117.
Prager, W., 1977b. Optimal arrangement of the beams of a rectangular grillage. In: Problemi Attuali di Meccanica e Applicata. Accademia delle Scienze, Torino, pp. 239–249.
Rasmussen, S.H., 1979. Optimization of fiber reinforced structures. Ph.D. Thesis, DCAMM Report No. S12, Dept. of Solid Mechanics, Technical University of Denmark, Lyngby, Denmark.
Rozvany, G.I.N., Zhou, M., Birker, T., 1992. Generalized shape optimization without homogenization. Struct. Optim. 4, 250–252.
Rozvany, G.I.N., Bendsøe, M.P., Kirsch, U., 1995. Layout optimization of structures. Appl. Mech. Rev. 48.
Rozvany, G.I.N., Adidam, S.R., 1972. Rectangular grillages of least weight. J. Eng. Mech. Div ASCE 98, 1337–1352.
Rozvany, G.I.N., Olhoff, N., Cheng, G., Taylor, J.E., 1982. On the solid plate paradox in structural optimization. J. Struct. Mech. 10, 1–32.
Thamburaj, P., Sun, J.Q., 2002. Optimization of anisotropic sandwich beams for higher sound transmission loss. J. Sound Vib. 254 (1), 23–36.
Sigmund, O., Torquato, S., 1997. Design of materials with extreme thermal expansion using a three-phase topology optimization method. J. Mech. Phys. Solids 45, 1037–1067.
Sigmund, O., 2001. Microstructural design of elastic band gap structures. In: Cheng, G.D., Gu, Y. (Eds.), Proc. of the 4th World Congress of Structrual and Multidisciplinary Optimization, WCSMO4, Dalian, China, June 4–8, 2001. Liaoning Electronic Press, Dalian, China, 6 pp.
Sigmund, O., Jensen, J.S., 2003. Systematic design of phononic band-gap materials and structures by topology optimization. Philos. Trans. Roy. Soc. London Ser. A 361, 1001–1019.
Sorokin, S.V., Olhoff, N., Ershova, O., 2006. The energy generation and transmission in compound elastic cylindrical shells with heavy internal fluid loading – from parametric studies to optimization. Struct. Multidiscip. Optim. 32, 85–98.
Stegmann, J., 2004. Analysis and optimization of laminated composite shell structures. Ph.D. Thesis, Dept. of Mechanical Engineering, Aalborg University, Aalborg, Denmark.
Stegmann, J., Lund, E., 2005. Discrete material optimization of general composite shell structures. Int. J. Numer. Meth. Eng. 62, 2009–2027.
Svanberg, K., 1987. The method of moving asymptotes – a new method for structural optimization. Int. J. Numer. Meth. Eng. 24, 359–373.
Taylor, J.E., 1975. Prediction of structural layout for maximum stiffness. J. Optim. Theory Appl. 15, 145–155.
Tcherniak, D., 2002. Topology optimization of resonating structures using SIMP method. Int. J. Numer. Meth. Eng. 54, 1605–1622.
Thomsen, J., Olhoff, N., 1990. Optimization of fiber orientation and concentration in composites. Control Cybernet. 19, 327–341.
Thomsen, J., 1991. Optimization of composite disks. Struct. Optim. 3, 89–98.
Tortorelli, D.A., Michaleris, P., 1994. Design sensitivity analysis: overview and review. Inverse Probl. Eng. 1, 71–105.
Wadbro, E., Berggren, M., 2006. Topology optimization of an acoustic horn. Comput. Meth. Appl. Mech. Eng. 196, 420–436.
Wang, C.M., Rozvany, G.I.N., Olhoff, N., 1984. Optimal plastic design of axisymmetric solid plates with a maximum thickness constraint. Comput. Struct. 18, 653–665.
Yamamoto, T., Maruyama, S., Nishiwaki, S., Yoshimura, M., 2008. Thickness optimization of a multilayered structure on the coupling surface between a structure and an acoustic cavity. J. Sound Vib. 318, 109–130.
Yoon, G.H., Jensen, J.S., Sigmund, O., 2007. Topology optimization of acoustic–structure interaction problems using a mixed finite element formulation. Int. J. Numer. Meth. Eng. 70, 1049–1075.